DANMARKS OG GRØNLANDS GEOLOGISKE UNDERSØGELSE RAPPORT 2011/52

Interpretation of geophysical data from the Tikiusaaq carbonatite

Report prepared for NunaMinerals A/S

T. M. Rasmussen

GEOLOGICAL SURVEY OF DENMARK AND GREENLAND
MINISTRY OF CLIMATE AND ENERGY

G E U S

DANMARKS OG GRØNLANDS GEOLOGISKE UNDERSØGELSE RAPPORT 2011/52

Interpretation of geophysical data from the Tikiusaaq carbonatite

Report prepared for NunaMinerals A/S

T. M. Rasmussen

Released 01.05.2015

GEOLOGICAL SURVEY OF DENMARK AND GREENLAND
MINISTRY OF CLIMATE AND ENERGY

GEUS

Contents

1. Executive summary

Geophysical data from the Tikiusaaq carbonatite are interpreted with focus on structural information from magnetic data. The interpretation is supplemented with inclusion of gamma-spectrometry data and remote sensing hyperspektral ASTER data.

The occurrences of magnetite sheets within the Tikiusaaq core complex are indentified clearly by the magnetic data. Modelling of the magnetic data indicates a depth extent of approximately 500 m or more. Strike and dip estimates are provided for a number of sheets.

Individual maps of gamma-ray spectrometry data (potassium, uranium and thorium) and minimum noise fraction (MNF) components of ASTER data are shown.

Correlations and relationships between magnetic data, gamma-spectrometry and ASTER data are analysed using a Self Organising Map approach. In general, the correlations are noted to be fairly complex. A classification based on a standard k-mean clustering analysis is provided, but no clear correspondence to outcrop observations is evident.

Interpretations of a possible extension of the carbonatite occurrence towards northwest of the previously defined core complex is put forward. The interpretation implies a somewhat larger extent that embrace the initial definition of the core complex. The new interpretation of possibly larger extent of the carbonatite must be viewed with some caution, and more geological data are needed to confirm or reject this interpretation.

2. Introduction

The discovery of the Tikiusaaq carbonatite in 2005 was guided by information from an analysis of stream sediment data, regional airborne magnetic data and radiometric data (Steenfelt *et al.* 2006). The carbonatite is associated with a strong magnetic signature at the centre of the intrusive complex and by low magnetisation within a zone surrounding the central region.

A detailed airborne magnetic and gamma-ray spectrometry survey was performed over the Tikiusaaq carbonatite and adjacent area by Sander Geophysics in 2010 on behalf of NunaMinerals A/S. Figure 1 shows the magnetic total field anomaly from the entire survey. This report presents an analysis of the magnetic data from the detailed airborne survey with a focus on providing structural information about the carbonatite complex. The report also includes a presentation of the gamma-spectrometry data and ASTER (Advanced Spaceborne Thermal Emission and Reflection Radiometer) data. The new magnetic and spectral data are analysed using a Self Organising Map (SOM) processing technique (Fraser & Dickson, 2007, Kohonen, 2001) which is suitable for an investigation of correlations between different data types. The SOM representation of the data is used to classify the area into regions of similar geophysical signature.

The extent of the carbonatite complex and carbonatite core as determined by Steenfelt et al. (2007) is marked on Figure 1. Two definitions are referred with respect the core: (1) defined from outcrop of carbonatite and (2) defined by the magnetic anomaly. These estimates of areal extent were based on previous regional geophysical data and field observations. A curved anomaly is seen immediately south of the outlined magnetic core. Thus, the the core of the complex is slightly larger towards south than the initial estimate. The interpretation of the extent of the carbonatite complex is discussed in more detail in chapter 7, where an interpretation involving a much larger extent is discussed.

The magnetic data from the survey have been utilised previously in a search for kimberlite rocks (Rasmussen, 2010). Figure 2a shows magnetic total field anomaly from a subset centred at the carbonatite (100 km^2 area) of the airborne survey. For comparison, the magnetic total field anomalies from surveys over the Sarfatoq and Qaqqaarsuk carbonatite complexes are shown in Figures 2b and 2c (data from Barnes, 2000a and 2000b). The three maps have identical lateral scale and the magnetic field is shown by using a similar data range (2000 nT and linear colour scale) for the magnetic field. A common feature is the high magnetic field values in the central zone and the weak magnetic field strength within an area surrounding the carbonatite, where magnetite in the host rocks has been destroyed by the thermal event. Differences in magnetic signatures are evident and may partly reflect differences in erosion levels.

Images of the radiometric data for the three surveys over the carbonatites are shown in Figure 3. Estimated concentrations of potassium, uranium and thorium are shown for the Tikiusaaq survey. No concentration estimates are available for the Qaqarssuk and Sarfartoq surveys and these data are presented as counts per second for the potassium, uranium and thorium detector windows. The images are therefore not fully comparable. However, the images clearly indicate differences in terms of peak locations for the anomalies of the radioactivity. In contrast to images of the magnetic field which is almost unaffected by quaternary cover deposits and water, the radiometric images only reflect properties of the top ½ m of the ground.

Figure 4 shows an image of the VNIR (visible near-infrared) ASTER data using a standard RGB colour scheme to represent the 3 short wavelength bands:

- Band 1; Blue colour, 520–600 nm
- Band 2; Green colour, 630–690 nm
- Band 3N; Red colour, 760–860 nm

The Aster data only reflect surface features. Any vegetation and water/snow will mask the geological signature.

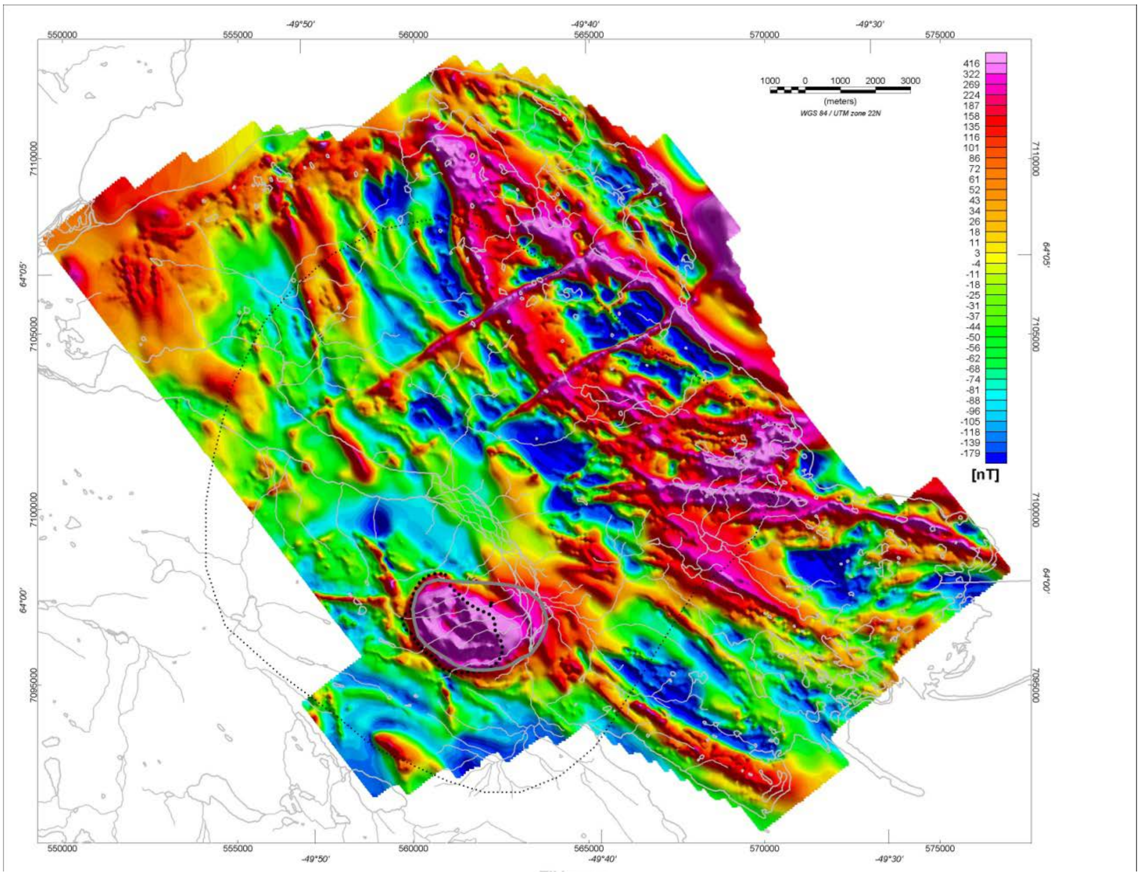

Figure 1. *Magnetic total field anomaly for the entire area covered by the geophysical survey by Sander Geophysics Ltd. in 2010. The two dashed polygons in black colour outline the carbonatite core (outcrop) and carbonatite complex respectively as defined by Steenfelt et al. (2007). The dark grey polygon outlines the magnetic core defined previously from regional aeromagnetic data.*

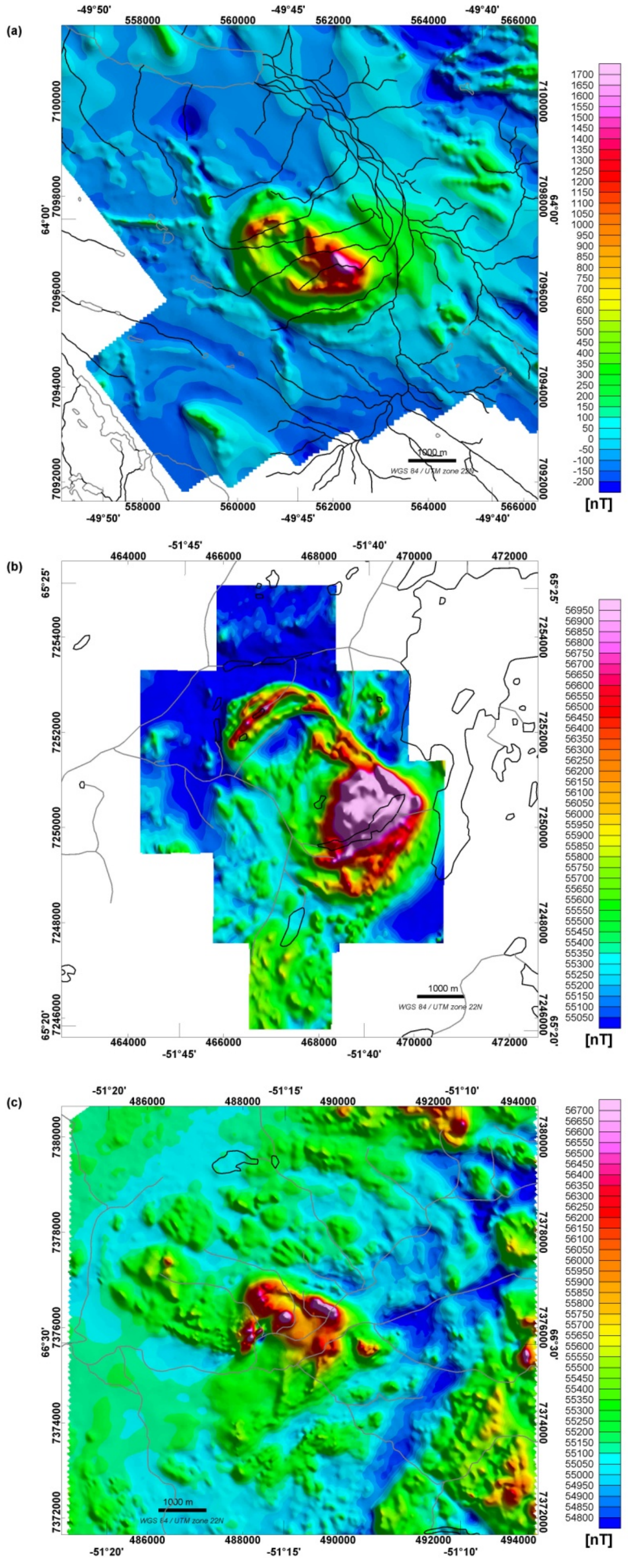

Figure 2. *(a) Magnetic total field anomaly for the Tikiusaaq carbonatite; (b) Magnetic total field for the Qaqqaarsuk carbonatite; (c) Magnetic total field for the Sarfartoq carbonatite. Rivers are shown by lines in grey colour and lakes are shown by polygons in black colour.*

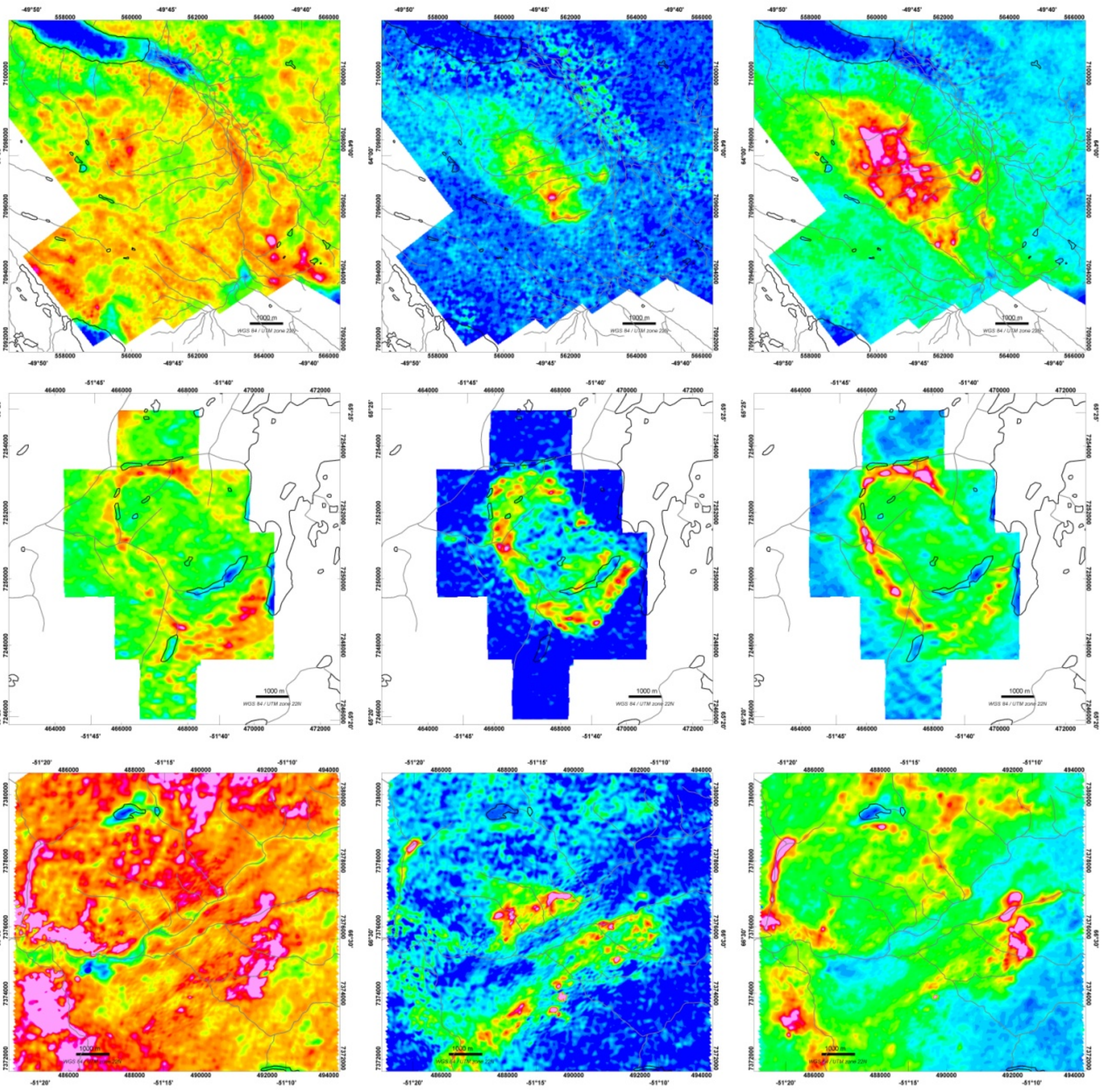

Figure 3. *The upper panel shows from left to right the estimated concentrations for potassium, uranium and thorium for the Tikiusaaq carbonatite. The area covered is identical to the area in Figure 2. The middle panel shows from left to right measured counts per second for the potassium, uranium and thorium windows respectively for the Qaqqaarsuk survey. The lower panel shows from left to right measured counts per second for the potassium, uranium and thorium windows respectively for the Sarfartoq survey. The measured counts per second for the Qaqqaarsuk and Sarfartoq surveys have not been converted to concentration values and the images for these areas are therefore not fully comparable to the images for the Tikiusaaq area. The colour coding is therefore somewhat arbitrary in this comparison (blue is low –red is high)*

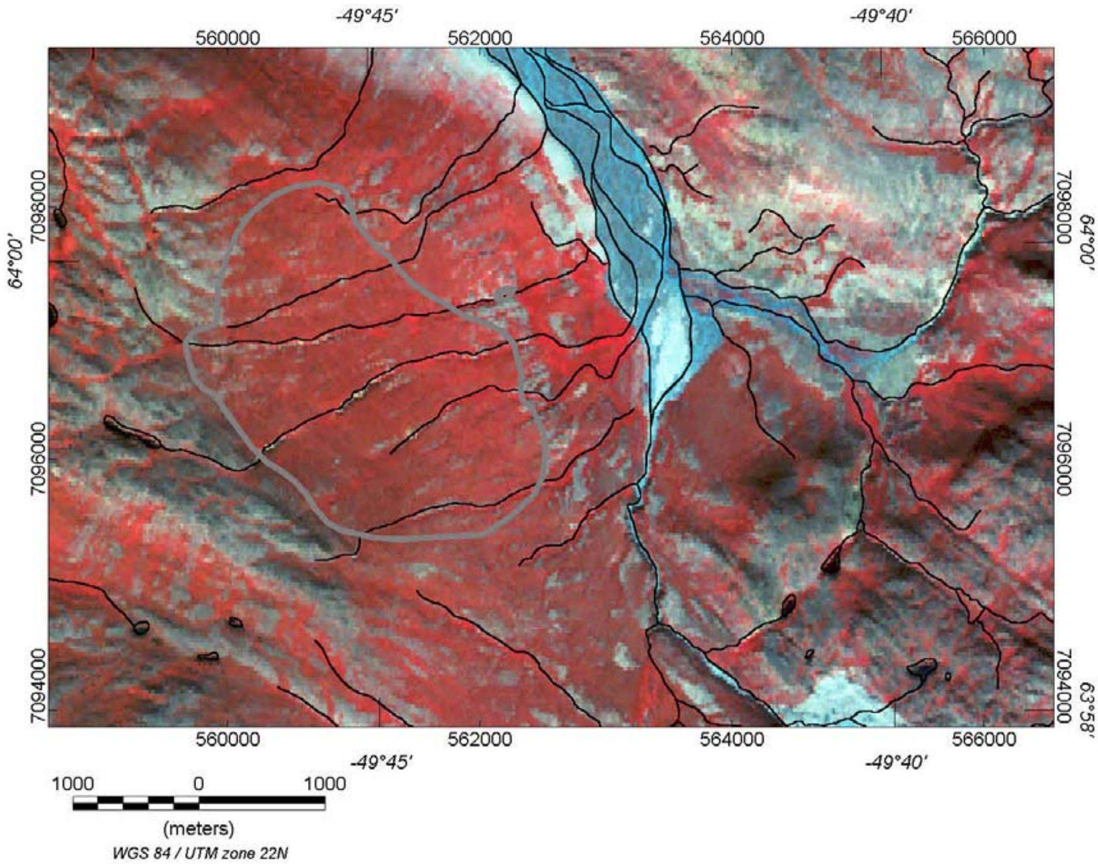

Figure 4. *Image of the first 3 spectral bands of the Aster data. The core of the carbonatite (defined by outcrop) outlined by Steenfelt et al (2007) is show by the polygon in grey colour. Rivers are shown by lines in black colour.*

3. Magnetic data

Structural information from the magnetic data is obtained by applying various processing techniques to the primary total magnetic field anomaly data. These techniques are generally applied to a grid representation of the magnetic total field anomalies and the results are presented as an image of the processed grid. Another approach is to model selected anomalies using either forward modelling or inversion techniques, in which model responses are compared to the measured data. In this report, results have been obtained using the inversion module available in the commercial Model Vision Pro software package from Encom Pty. Ltd. The structural information obtained from the grid images is used to guide the choice of principal model used in the inversion; e.g. a choice of strike direction and strike length for dykes or sheet like structures.

3.1 Structural information from grid images

Most of the methods used for extracting structural information from the grids of measured magnetic field data involve enhancement of short wavelength features relative to features with long wavelength. Typical processing filters involve some sort of differentiation, either in horizontal direction or in vertical direction. Differentiation may be applied directly to the total magnetic field intensity or to other transformed data of these. In this report we apply differentiation to the pseudo gravity field and to the magnetic tilt angle. The pseudo gravity field transformation of the magnetic field intensity simplifies the interpretation, because the magnetic field anomalies, which always have both positive and negative parts, are transformed into a single peak anomaly. The tilt angle transformation calculates the angle between the vertical and horizontal derivatives of the magnetic field. The advantage of the tilt-angle calculation is that structures with low magnetisations are still visible in the final image. The images included are as follows:

- Magnetic total field intensity (Figure 5)
- Second vertical derivative of magnetic total field intensity (Figure 6)
- Pseudo gravity field (Figure 7)
- Second vertical derivative of pseudo gravity field (Figure 8)
- Magnetic tilt angle (Figure 9)
- Horizontal gradient of magnetic tilt angle (Figure 10)

The association of the carbonatite core with sheets of high magnetisations is evidenced in all maps displayed in Figures 5-8. Note that the colour scale representation in Figure 5 is based on an equal area representation and that this differs from the linear scale representation used in Figure 2. The equal area representation provides a better visualisation of subtle features and local variations compared to the use of a linear scale. The linear representation emphasizes locations of high magnetisation. The approximate locations of highly magnetised sheet structures are marked in Figure 8. The polygon boundaries outline the projection of the top of the sheet structure to the surface position. Estimates of geometry details (dip, thickness, depth to top and bottom) are discussed in the chapter below on inversion of profile data. The boundary drawings are partly based on lineaments derived from the horizontal gradient of the second vertical gradient of the pseudo gravity field by using a semi automatic “edge” detection technique (Kovesi, 1999). The technique finds locations with high gradient (“edges”) in the input data; i.e. in this case the locations with a high gradient of the horizontal gradient of second vertical gradient data.

The boundary drawings in Figure 8 include two features indicating strong magnetisation northwest of the carbonatite core outlined by Steenfelt et al. (2007). The interpretation of the southernmost east-west trending anomaly is that this is caused by a dolerite dyke. A dolerite dyke has been reported at this location at three sites (Steenfelt et al. 2007). A width of 40 m for the dyke is quoted by Steenfelt (2011; personal communication). The origin of the north-south trending anomaly is uncertain, but a dolerite dyke is reported at one locality adjacent to the anomaly. Inspection of the geological map in scale 1: 100 000 (Geologisk Kort over Grønland, Kapisillit 64 V.2 SYD) indicates exposures of othopyroxene bearing gneiss and anothosites within this area. The pattern of the magnetic anomalies between the two major anomalies and within the adjacent areas south and east of the two anomalies has some similarities with typical responses associated with carbonatite intrusions. The field strength is however notably lower than for the core area. The similarity may be an indication of a much larger north-westerly extension of the carbonatite than estimated initially. The possibility of an enlarged area with carbonatite is discussed in more detail in chapter 7 with reference to Figure 36, which contains detailed maps of magnetic and gamma spectrometry data concerning this particular interpretation.

The magnetic tilt angle data (Figure 9-10) facilitate detection of structures in areas of low magnetic intensity, which are not clearly seen in the other images that depends linearly on magnetisation. Superimposed on the image of the horizontal derivative of the tilt angle are major lineaments that are defined by boundaries between areas of different texture for the anomaly appearance or where anomalies are truncated or offset. The lineaments have been drawn by visual inspection of the images.

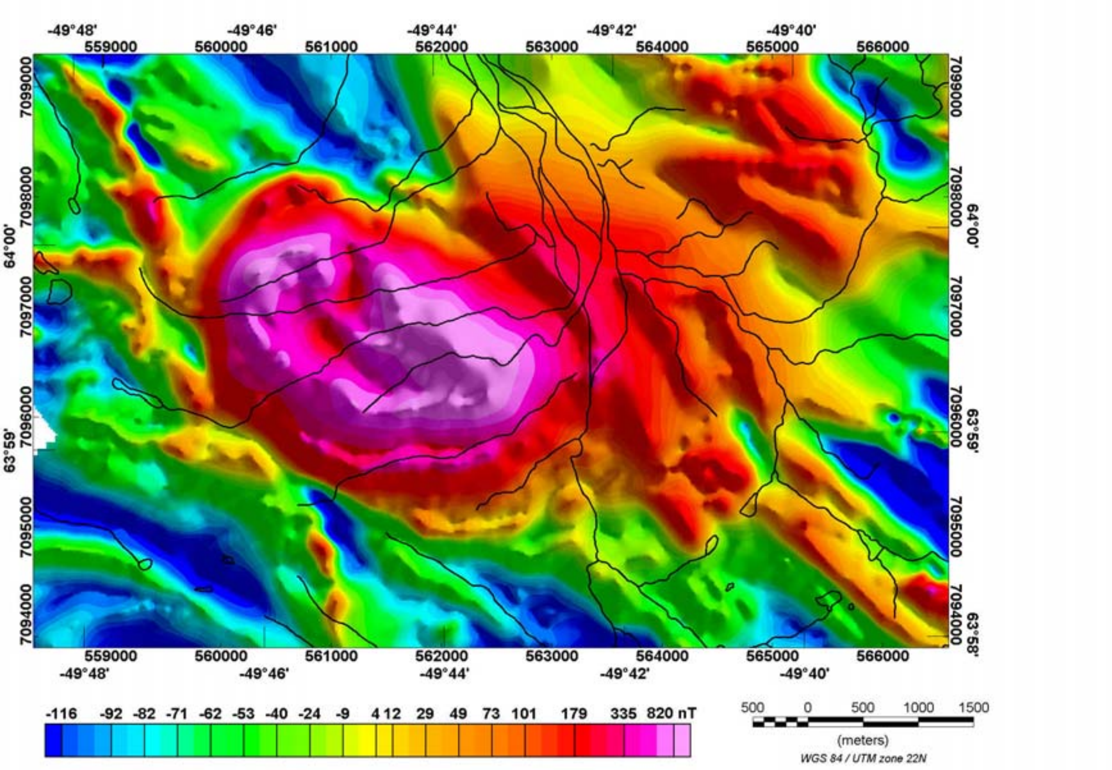

Figure 5. *Magnetic total field intensity in the area of the carbonatite core.*

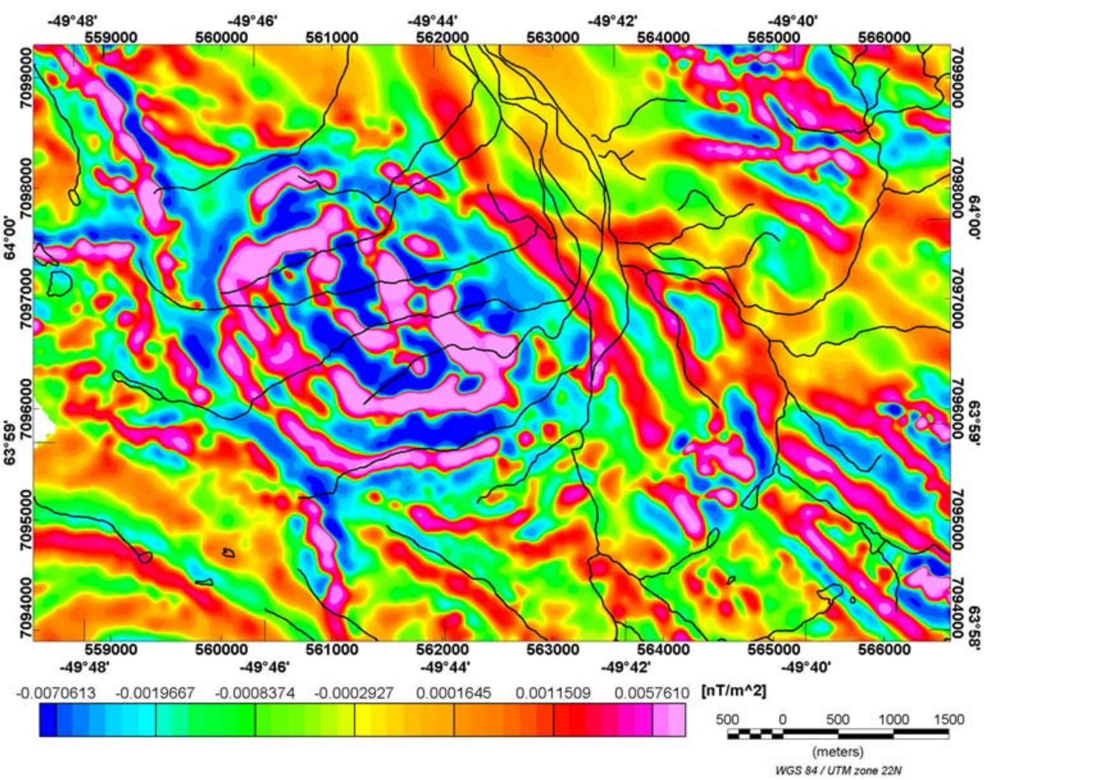

Figure 6. *Second vertical derivative of magnetic total field intensity in the area of the carbonatite core.*

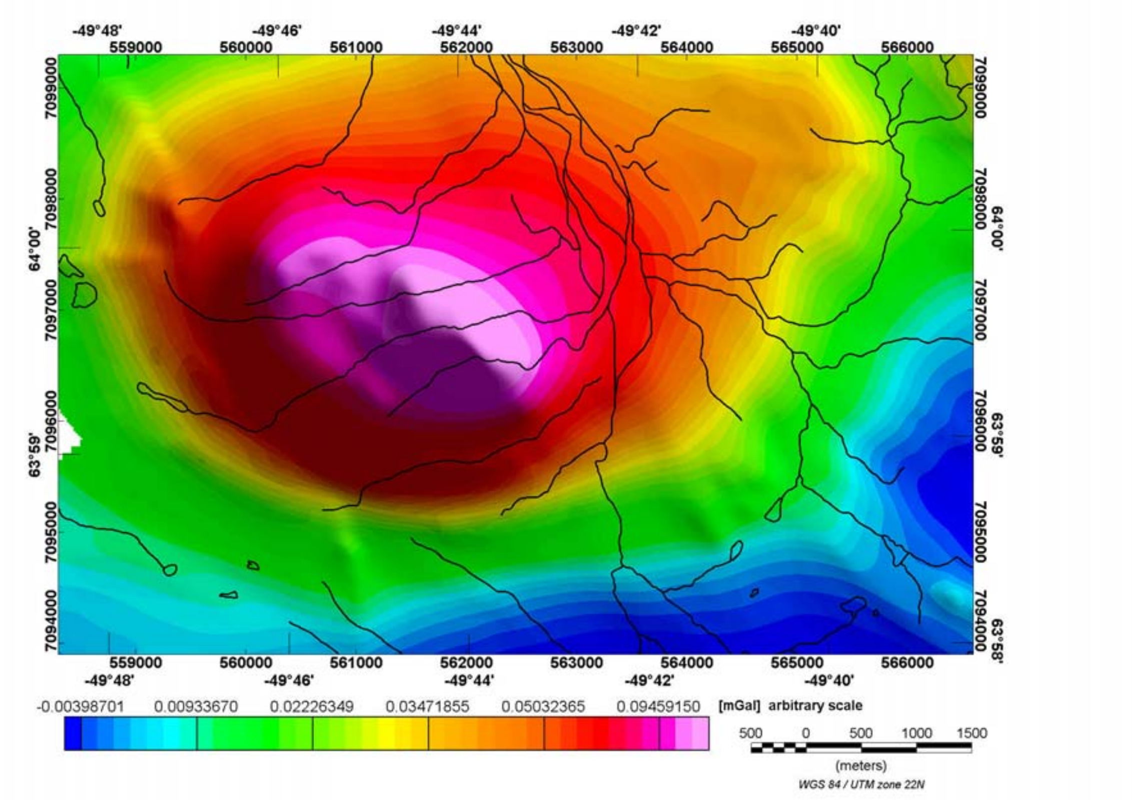

Figure 7. *Pseudo gravity field in the area of the carbonatite core.*

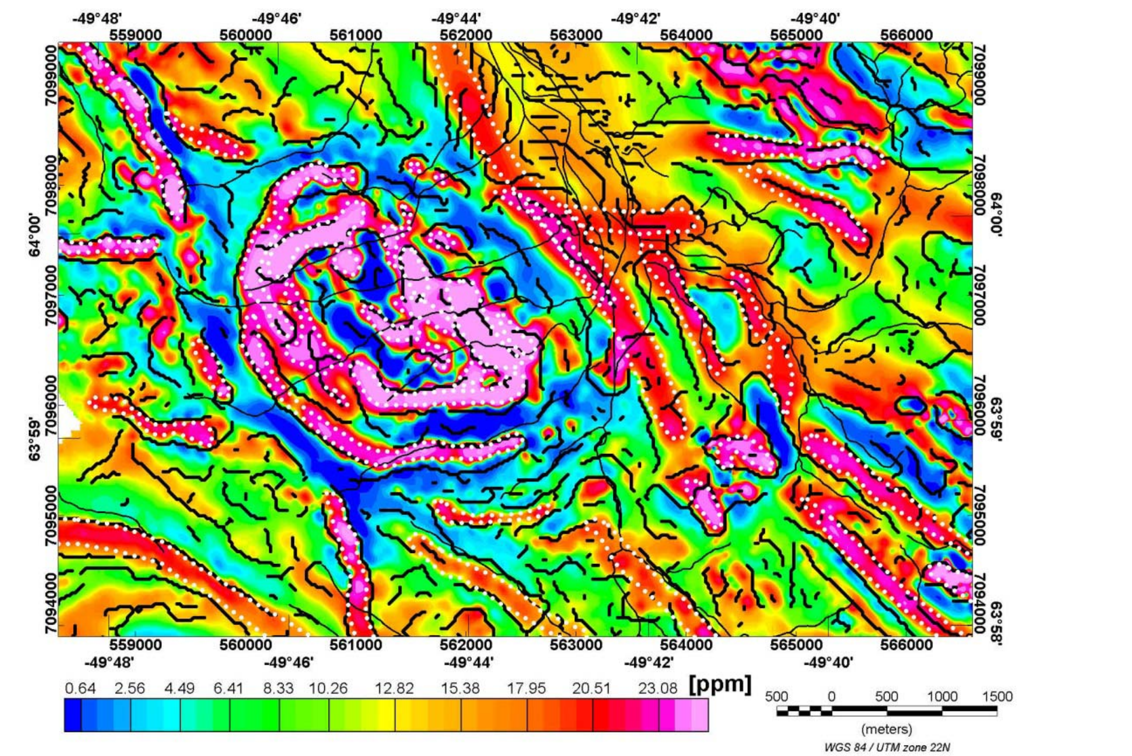

Figure 8. *Second vertical derivative of the pseudo gravity field in the area of the carbonatite core. Thick black lines mark location of high horizontal gradients found by using the "edge" technique of Kovesi (1999). Dotted white polygons mark the approximate boundaries for high magnetic structures used in modelling.*

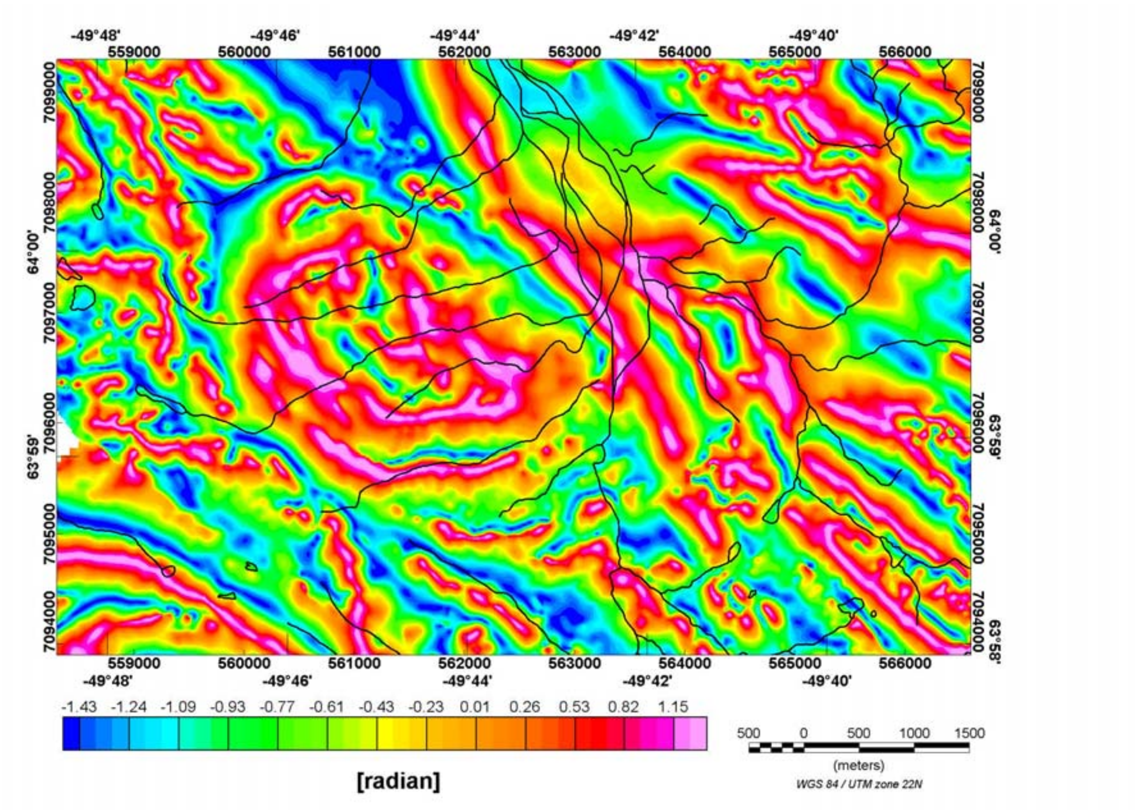

Figure 9. *Magnetic tilt angle in the area of the carbonatite core. Peak values mark approximate location of magnetic structures.*

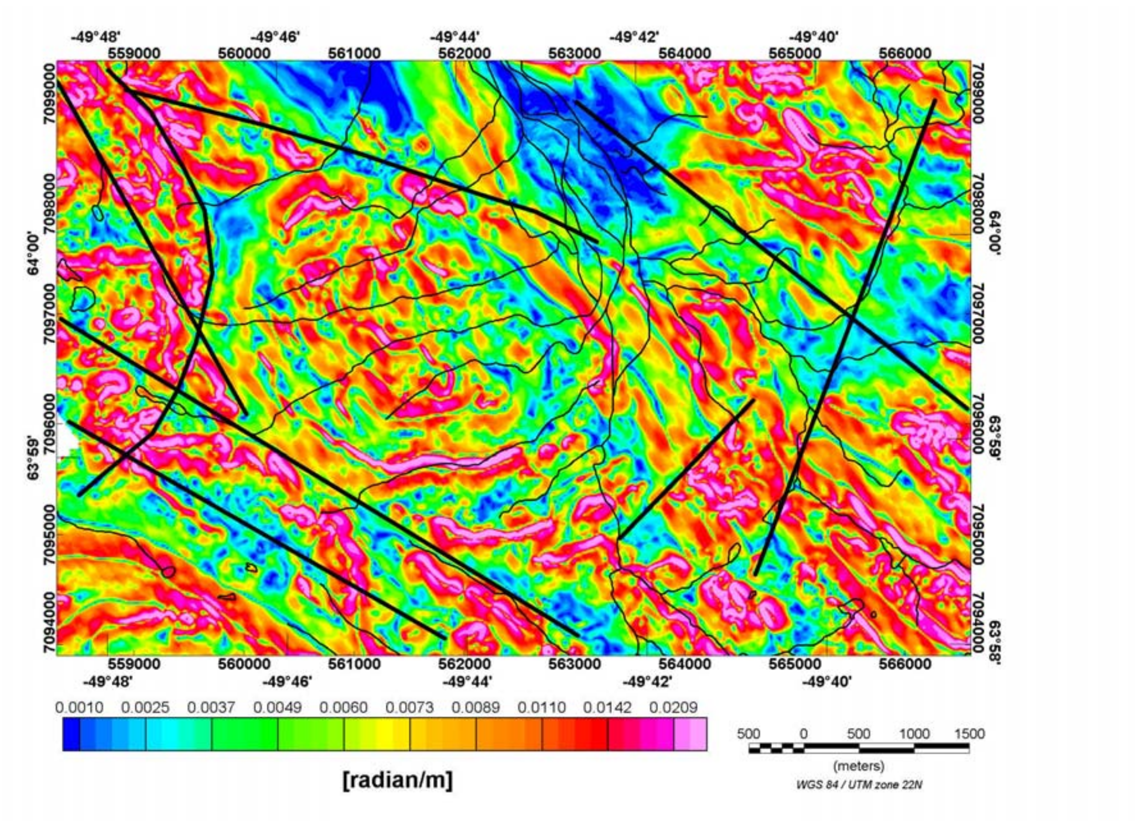

Figure 10. *Horizontal gradient of magnetic tilt angle in the area of the carbonatite core. Linear features with zero values (dark blue colour) mark approximate position of magnetic structures. Thick black lines mark location of inferred structural break.*

3.2 Structural information from inversion of data

Structural information is derived from the measured magnetic total field data by applying an inversion technique available from the commercial software ModelVision Pro. The technique includes the following steps:

- Selection of a subset of data for interpretation
- Selection of principal model; e.g. dyke, sphere or ellipsoid as causative body
- Select which parameters for the model shall be kept fixed during inversion and which parameters to search for
- Automatic adjustment of parameters until an acceptable fit been measured and model responses is achieved

Data from five profiles have been selected for inversion (Figure 11). Two of these are actual measured data along survey flight lines (lines 118 & 119), whereas the other three are extracted data from the interpolated and gridded total field data (grid profiles 1-3).

(a)

(b)

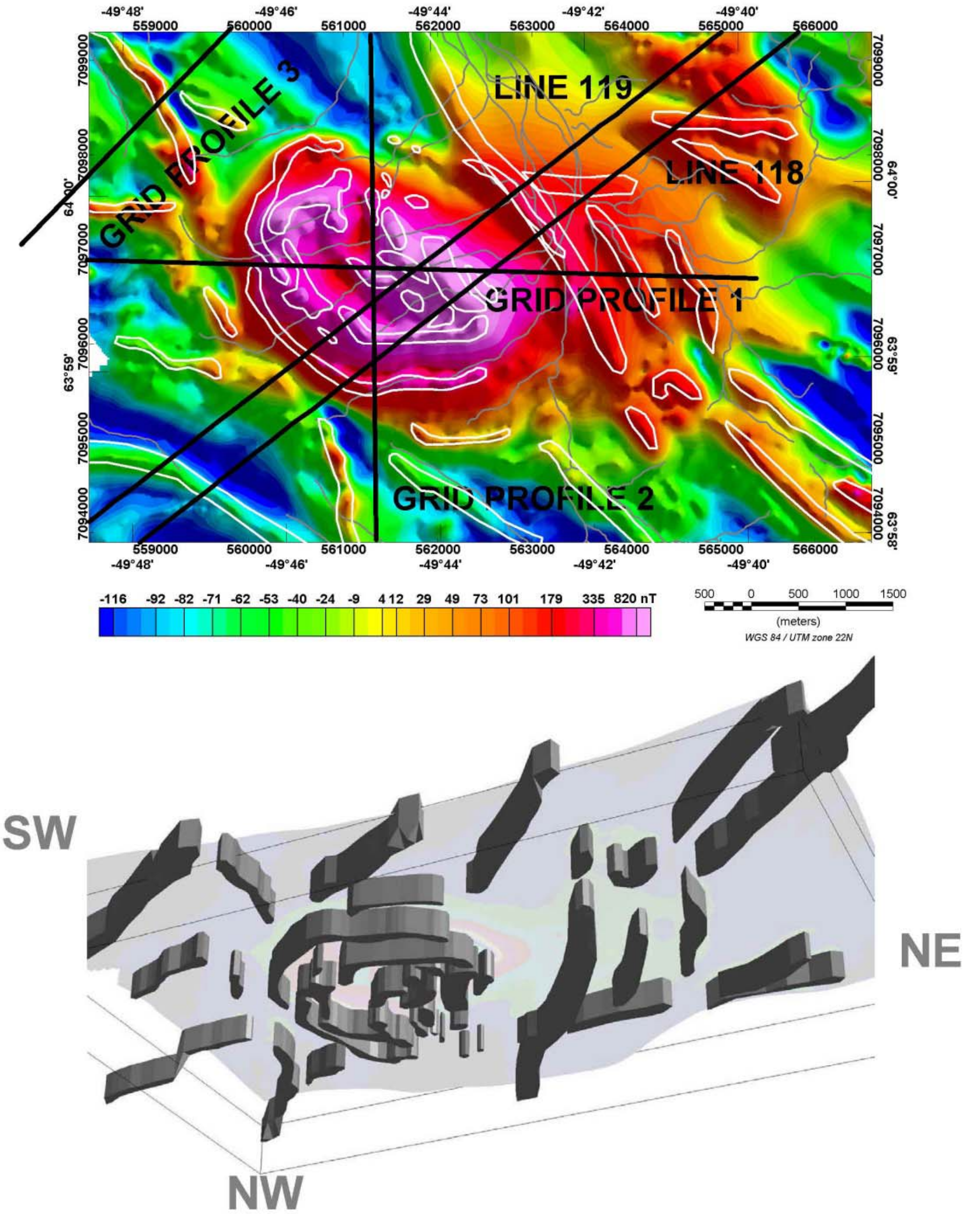

Figure 11. *(a) Location of profiles selected for data inversion. Lines 118 and 119 are two flight lines and grid profiles 1–3 correspond to data extracted from interpolated and gridded magnetic data. Polygons in white colour show approximate locations of boundaries for highly magnetised bodies. (b) Perspective view of highly magnetised bodies seen from below. The dips of the bodies are all shown as vertical and the image is only a schematic representation of the likely occurrence of highly magnetised bodies.*

All interpretations used for this report is based on a tabular body as principal model (Figure 12). This model can approximate both dykes and more localized structures. The model parameters for each body are:

- Susceptibility
- Depth to top
- Length along strike
- Width

- Depth extent
- Depth to top
- Dip
- Azimuth or strike direction

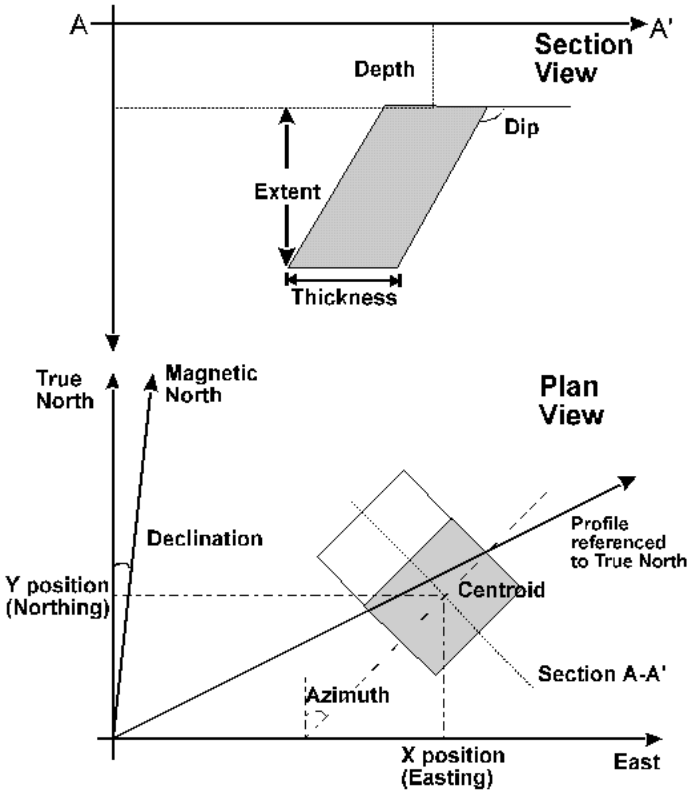

Figure 12. *Principal model used for inversion of data (Figure from Encom Model Vision Reference Manual by Pitney Bowes Pty Ltd).*

The number of tabular bodies for each profile and the corresponding strike directions are obtained directly from visual inspection of the images in Figure 8 and 11a. The strike direction is treated as a fixed parameter in the inversion of the data. Figure 11b represents a schematic perspective view (seen from below) of the highly magnetised structures, and it is clear that the use of tabular bodies to model the data is a simplification in relation to the complexity of structures.

Modelling of magnetic data is known to be highly non-unique; i.e. several models can produce the same magnetic response. Some of these models can be disregarded due to unrealistic physical properties, such as extreme susceptibility, but non-uniqueness still remains after rejection of these extreme models. In particular, dyke models having similar thickness·susceptibility product will have almost identical responses and it is not possible to discriminate between these models within a fairly large range of thickness and susceptibility values. Another complication in modelling magnetic data is that features at large depth are subject to large uncertainties. It is usually difficult to provide information with confidence about the deeper part of the structures.

Measured and model responses and the corresponding models along profiles 118 and 119 are shown in Figure 13 and 14 respectively. Profiles 118 and 119 are parallel and the distance between the lines is 500 m. The responses show some similarity but differences in both shape and amplitude can be seen. The differences in data are reflected in the differences in model parameters, but the aforementioned non-uniqueness, when modelling the data, may also contribute to the differences. Model parameters are listed in Tables 1 and 2 respectively. Results from modelling of data along grid profiles 1–3 are shown in Figure 15–17 and listed in Tables 3–5.

Most of the obtained susceptibility values are in the order of 0.2-0.5 SI, which is about an order of magnitude less than values for pure magnetite. In general, dyke models for which the susceptibility thickness product is similar have almost identical responses and the actual susceptibility and thickness are therefore not well determined. The tabulated thickness estimates might therefore be somewhat larger than the actual thickness of magnetite bodies. Although exceptions exist, the structures are dipping outwards and away from the centre of the core complex. The continuation of the dyke-like structures at depth is not well determined and the data do not provide information with much confidence on the actual geometry. However, many of the dykes have a large depth extent (> 500m) which is an indication of continuity to fairly large depth of the structure.

The estimates of depths to the top of the structures are in most cases somewhat below the surface. The implication of this is not straightforward to evaluate. Theoretically, it is possible to force all dyke models to be exposed at the surface and still obtain a good fit between measured and model responses. These models will have smaller volumes of the dykes than displayed in Figures 13–17, but their extension to large depth is still likely.

The structure labelled no. 2 in Figure 17 along grid profile 3 is most likely caused by a dolerite dyke, as discussed in chapter 3. The thickness estimate of 2m is however much smaller than the quoted thickness of about 40 m. The reason for this discrepancy is attributed to a model susceptibility with an order of magnitude larger than the in-situ value of 0.04SI quoted by Steenfelt (2001, personal communication).

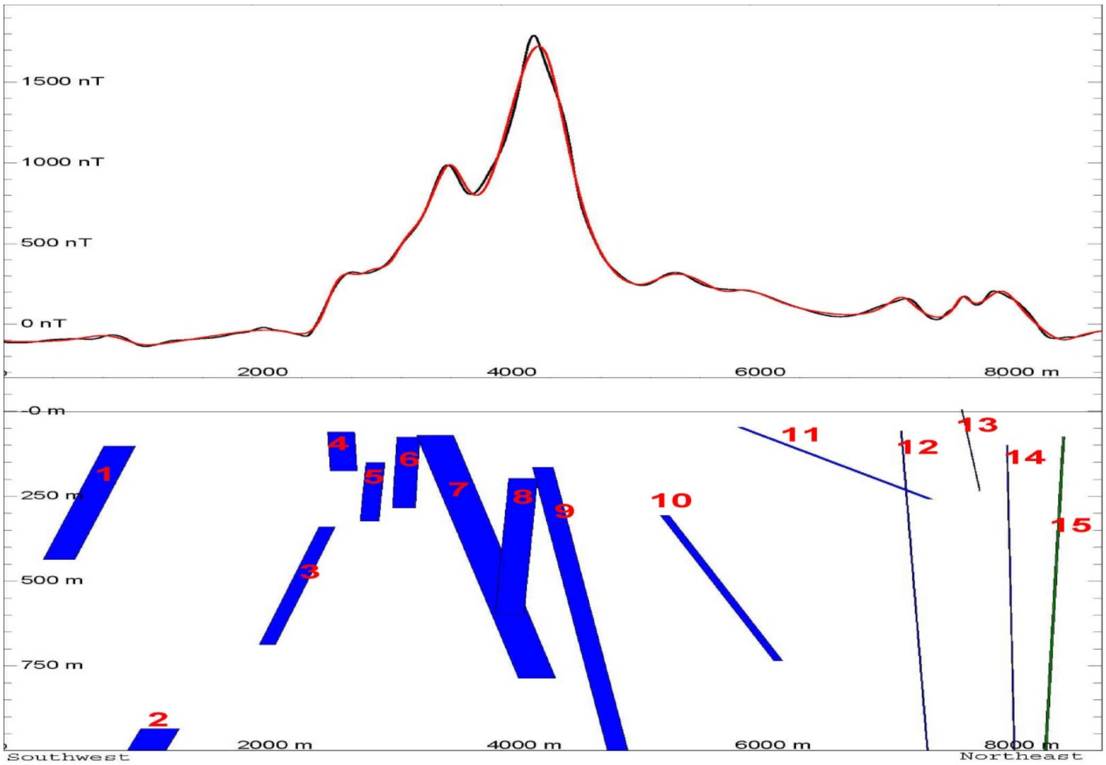

SW NE

Figure 13. *Black and red curves in the upper panel shows measured and model response respectively along profile 118. The lower panel show a cross section through the corresponding model.*

Table 1. *Properties for model in Figure 13 along line 118. All units are in SI.*

Body no.	Susceptibility	Width	Depth top	Depth ex-tent	Dip	Azimuth
1	0.014	233	103	334	143	-60
2	-0.11	285	935	2732	147	-60
3	0.14	95	340	347	136	-80
4	0.07	214	60	116	80	-45
5	0.21	150	150	173	105	-37
6	0.11	184	75	209	100	-38
7	0.14	296	70	716	41	-37
8	0.22	231	197	400	105	-38
9	0.3	166	165	1628	54	-38
10	0.5	69	306	429	25	-38
11	0.54	37	47	219	8	-38
12	0.29	8	58	1912	81	-80
13	0.23	5	0	250	66	-80
14	0.81	7	99	1120	87	-80
15	-0.1	20	75	1234	99	-38

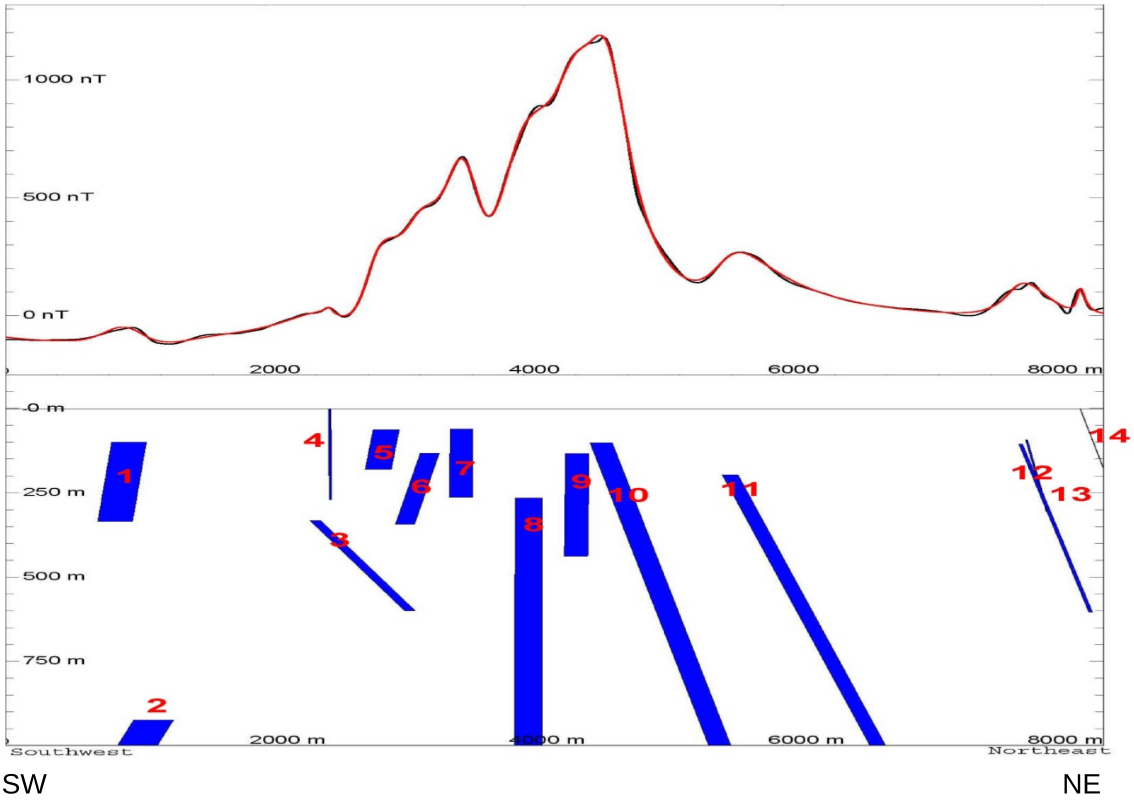

Figure 14. *Black and red curves in the upper panel shows measured and model response respectively along profile 119. The lower panel show a cross section through the corresponding model.*

Table 2. *Properties for model in Figure 14 along line 119. All units are in SI.*

Body no.	Susceptibility	Width	Depth top	Depth extent	Dip	Azimuth
1	0.014	247	99	236	113	-60
2	-0.11	282	925	1732	147	-60
3	0.34	59	332	268	26	-60
4	0.01	13	0	270	89	-80
5	0.061	198	62	118	117	-45
6	0.21	145	132	211	132	-37
7	0.12	177	61	203	91	-37
8	0.27	201	266	1082	90	-37
9	0.19	181	134	305	92	-38
10	0.21	102	102	1381	44	-38
11	0.13	119	196	1489	35	-38
12	0.2	20	105	499	51	-80
13	0.05	11	93	213	61	-80
14	0.31	1.5	0	1044	53	-80

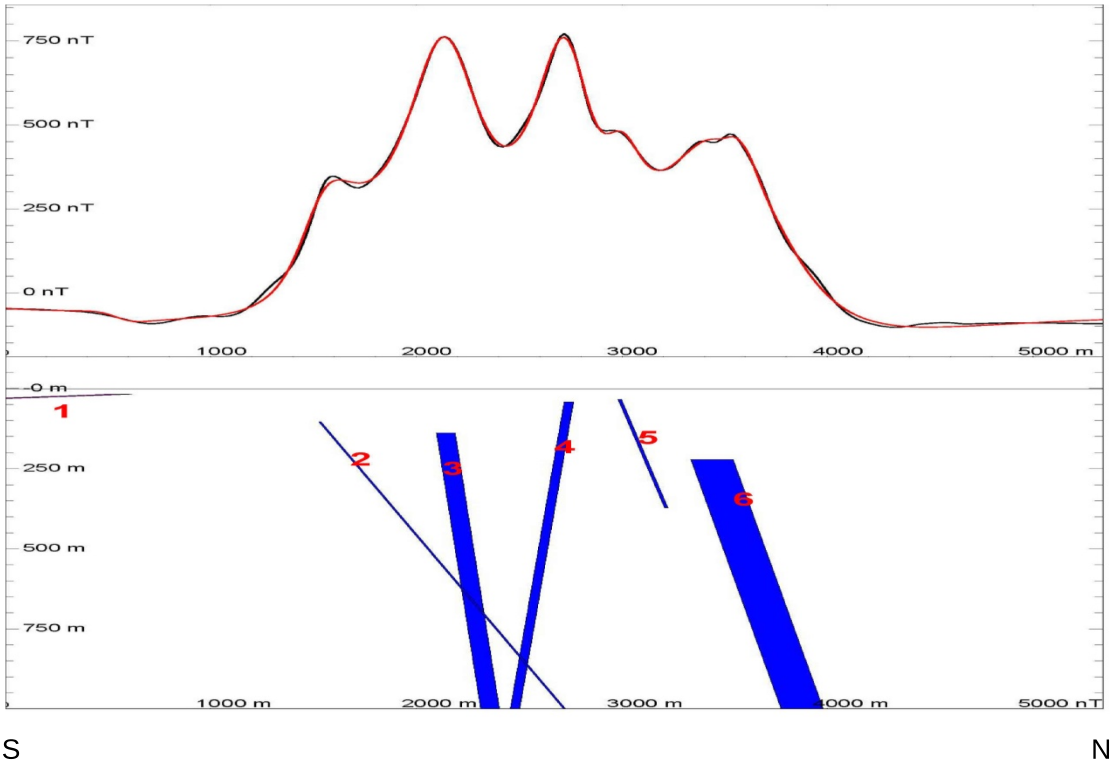

Figure 15. *Black and red curves in the upper panel shows measured and model response respectively along grid profile 1. The lower panel show a cross section through the corresponding model.*

Table 3. *Properties for model in Figure 15 along profile 1. All units are in SI.*

Body no.	Susceptibility	Width	Depth top	Depth extent	Dip	Azimuth
1	0.13	120	18	16	178	269
2	1.2	10	104	2463	143	90
3	0.23	91	138	1280	76	269
4	0.39	31.9	42	1312	101	-45
5	0.38	14	33	339	60	-60
6	0.22	143	222	822	68	-45

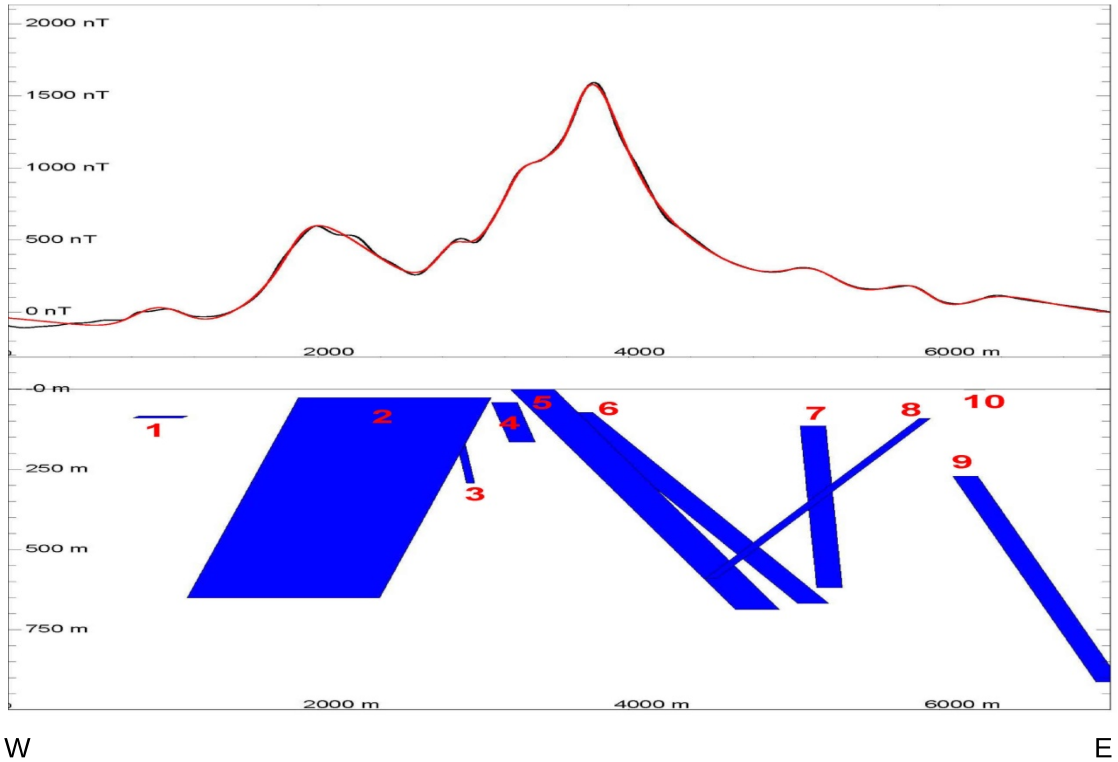

Figure 16. *Black and red curves in the upper panel shows measured and model response respectively along grid profile 2. The lower panel show a cross section through the corresponding model.*

Table 4. *Properties for model in Figure 16 along profile 2. All units are in SI.*

Body no.	Susceptibility	Width	Depth top	Depth extent	Dip	Azimuth
1	0.4	214	83	7	165	-45
2	0.05	850	27	624	128	-45
3	0.23	36	45	248	71	-45
4	0.55	79	42	123	66	-60
5	0.13	192	0	687	34	-45
6	0.54	135	72	595	30	-45
7	0.06	112	114	505	82	-45
8	0.33	48	91	500	152	-45
9	0.22	109	271	642	45	-45
10	-0.09	83	0	1	0.5	-45

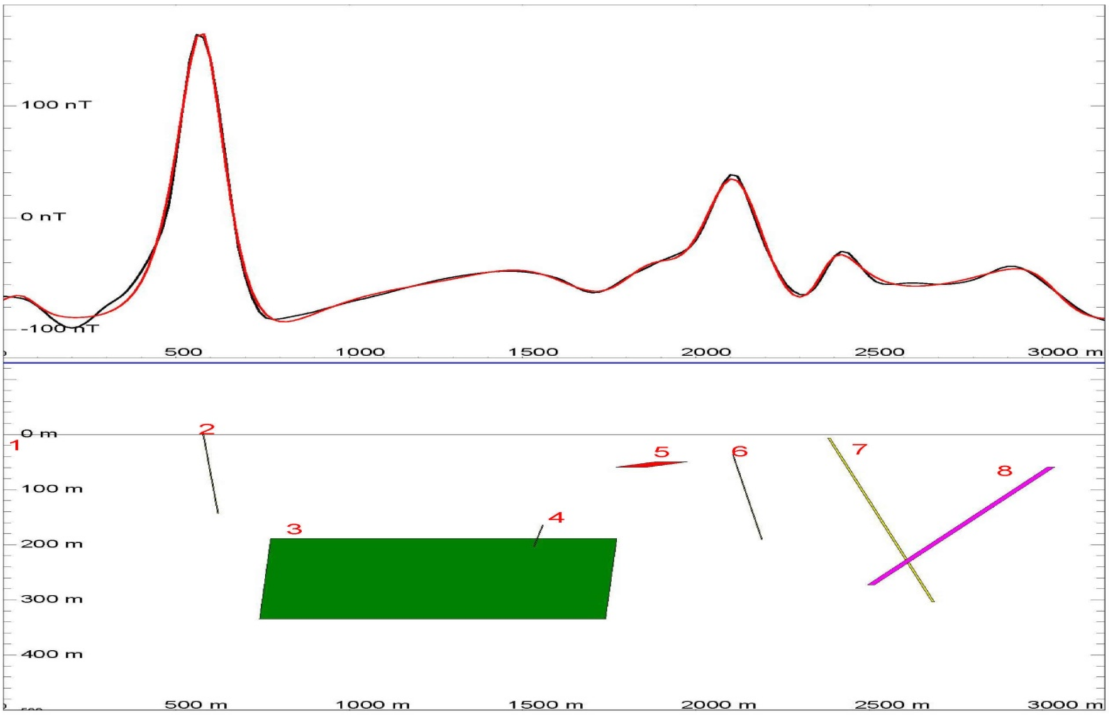

SW NE

Figure 17. *Black and red curves in the upper panel shows measured and model response respectively along grid profile 3. The lower panel show a cross section through the corresponding model.*

Table 5. *Properties for model in Figure 17 along profile 3. All units are in SI.*

Body no.	Susceptibility	Width	Depth top	Depth extent	Dip	Azimuth
1	2.1	3.8	0	1.7	163	-80
2	2	1.9	0	148	76	-80
3	0.008	998	189	145	10	-45
4	2.18	1.7	163	39.8	118	-80
5	0.11	91	49	10	175	-45
6	2	1.8	36	154	66	-80
7	0.2	6	6	297	45	-46
8	0.12	19.3	59	214	158	-46

4. Gamma-spectrometry data

Maps of the estimated concentrations of potassium, uranium and thorium are displayed in Figures 18–20 and the ternary image of all elements is shown in Figure 21. Boundaries for the highly magnetic structures are shown on the maps. The co-existence of an anomalous gamma-spectrometry variation and magnetic variations is clear. Note, however that the locations with maximum thorium and uranium values are seen to coincide with areas of low to intermediate magnetic field variation. A correlation/anti-correlation is not very clear and some of the locations with intermediate to high uranium and thorium concentrations coincide with locations of high magnetic field strength. The distribution of estimated concentrations as functions of the magnetic field is illustrated in Figure 22, which shows concentrations versus the second vertical derivative of the magnetic field at the locations, where the magnetic field has a local peak. The complex relationship between magnetic field variations and the gamma-spectrometry data are discussed in the section with Self Organising Maps.

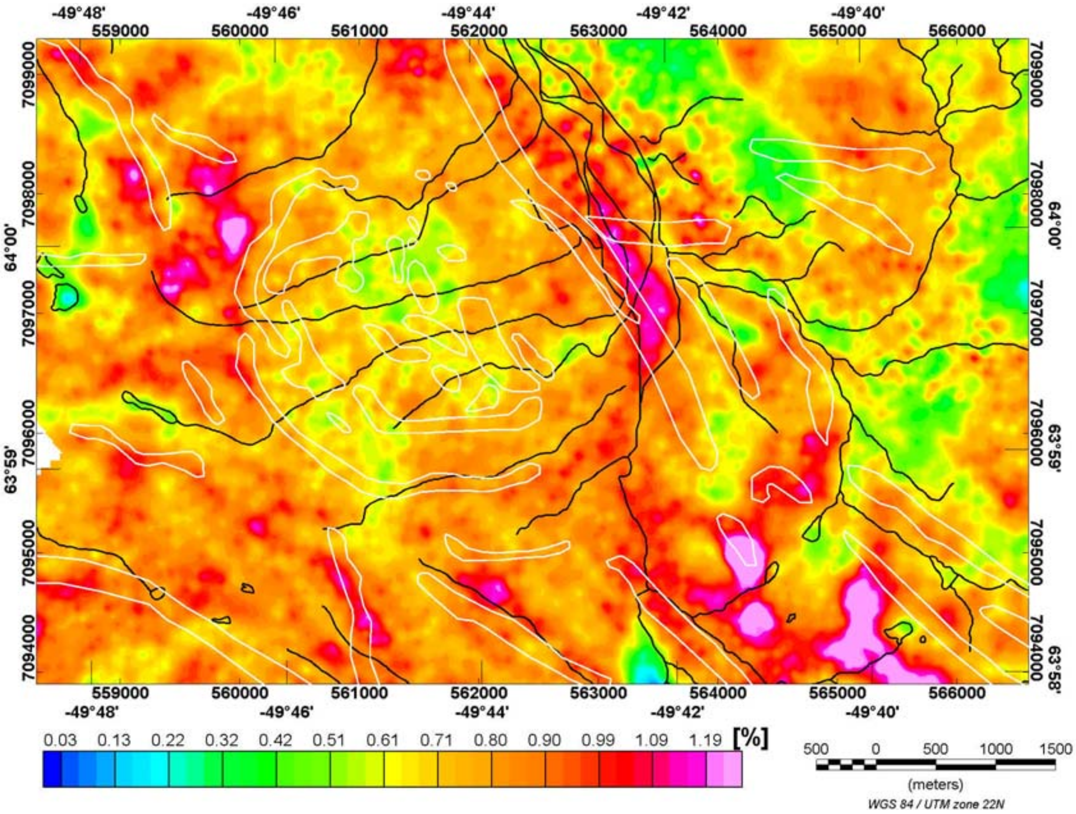

Figure 18. *Estimated pottasium concentration. Polygons in white colour outline major magnetic structures-*

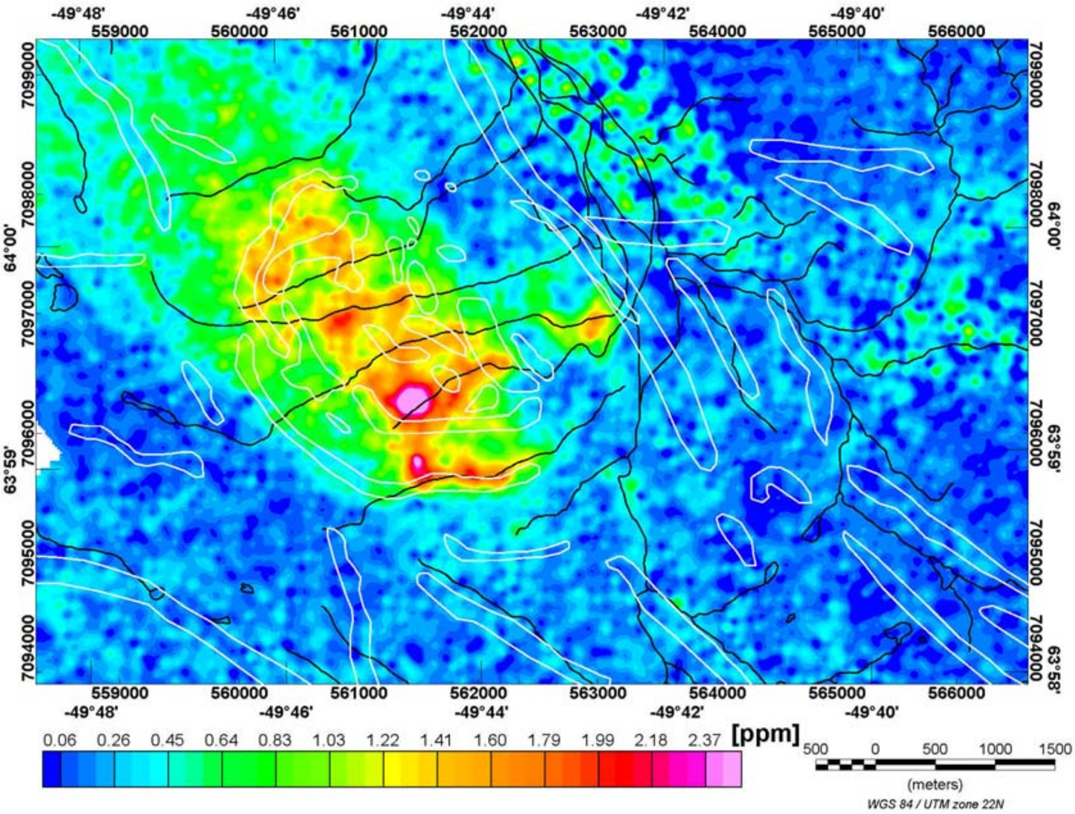

Figure 19. *Estimated uranium concentration. Polygons in white colour outline major magnetic structures-*

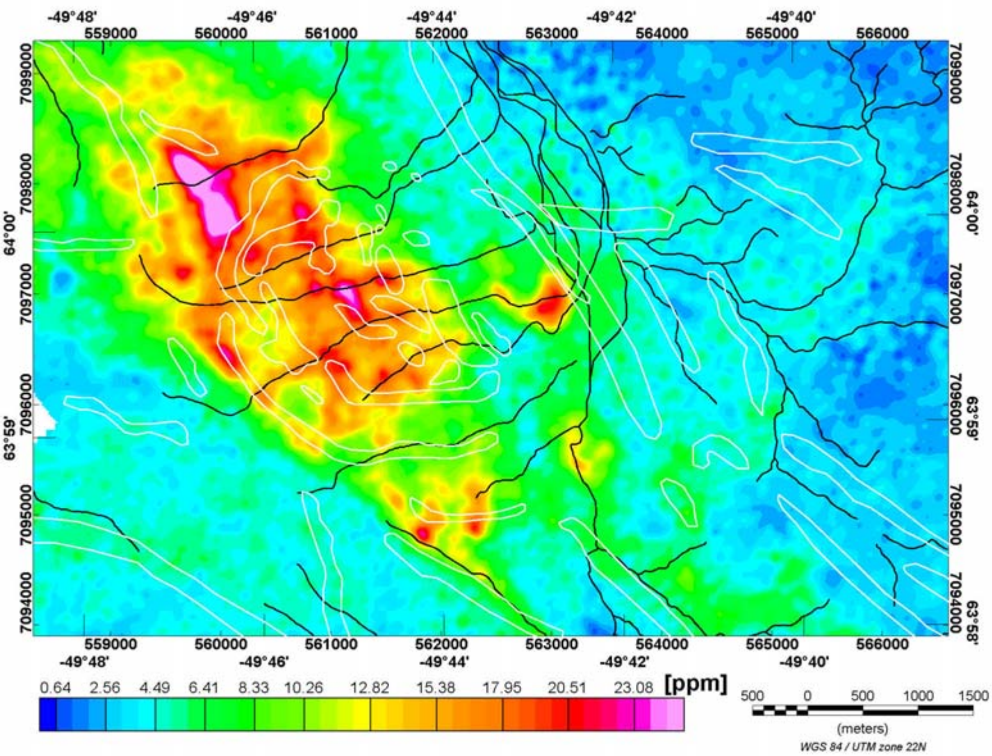

Figure 20. *Estimated thorium concentration. Polygons in white colour outline major magnetic structures.*

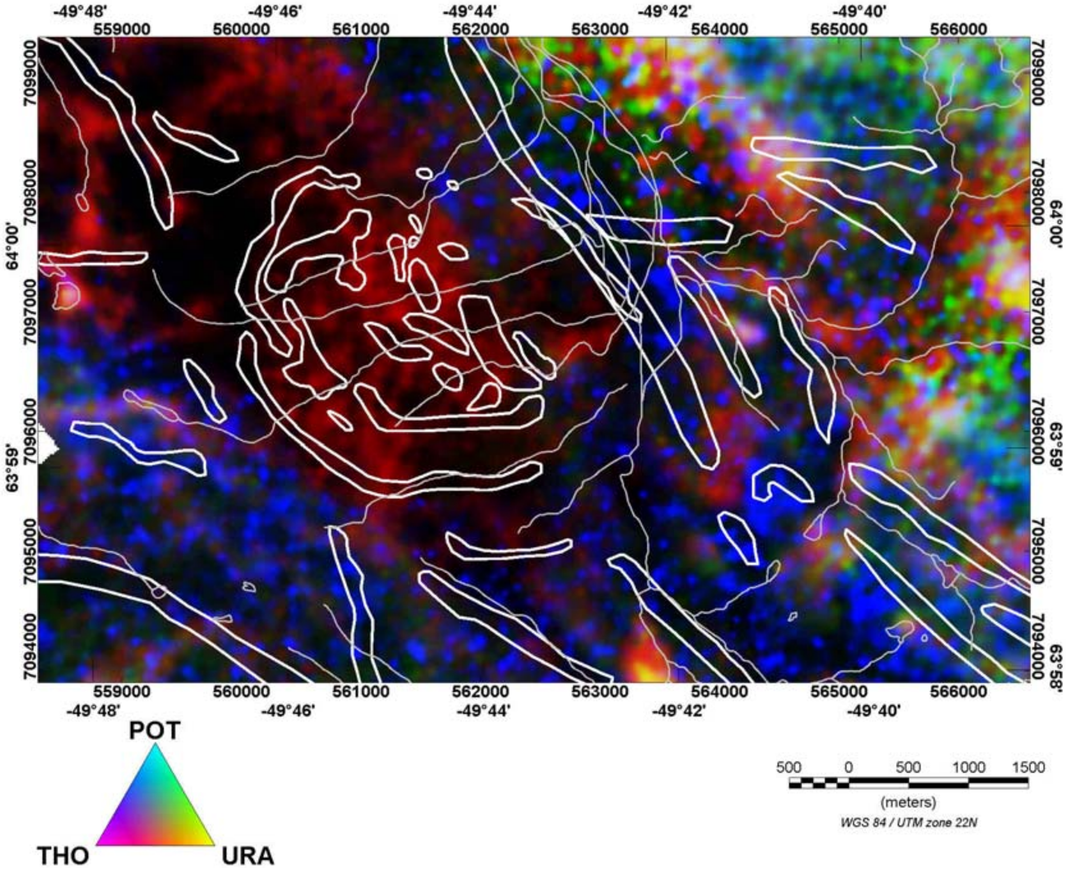

Figure 21. *Ternary image of gamma-spectrometry data. Polygons in white colour outline major magnetic structures-*

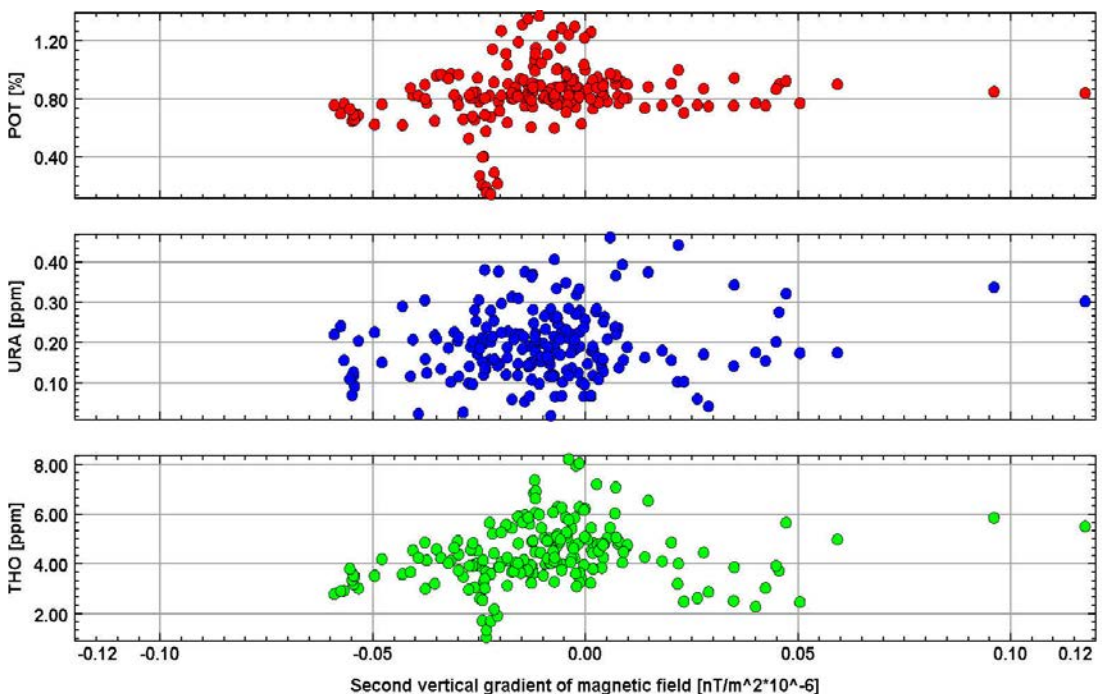

Figure 22. *Relationships between the second vertical derivative of the magnetic field and estimated concentrations of potassium, uranium and thorium. The data are selected at locations where the second vertical derivative of the magnetic field as local maxima.*

5. Aster data

The report by Steenfelt et al. (2007) includes a presentation and interpretation of ASTER data from the Tikiusaaq area. The data were presented using a standard RGB image representation of the VNIR (visible near-infrared) reproduced here in Figure 4. In order to facilitate further use of the ASTER data, images of the minimum noise fraction (MNF) decomposed data are presented in Figures 23–31. The MNF decomposition (Green *et al.* 1988) separates the data into a number of spectral bands, which to some degree place focus on different properties of the ground. The transformation splits the data into de-correlated data. The spectral components 1–9 are ranked according to noise content. The amount of noise increases with increased component number, a characteristic that is easily recognised in the images in Figures 23–31. The images may be used as a first order classification of the area in terms of similarity of ASTER data and thereby properties of the ground. In particular MNFcomponents 2–4 outline the carbonatite core, but also components with higher numbers are seen to provide independent information, which is useful for further sub-division of the area. An automated classification or clustering of the ASTER data is provided in the section on Self Organised Map analysis.

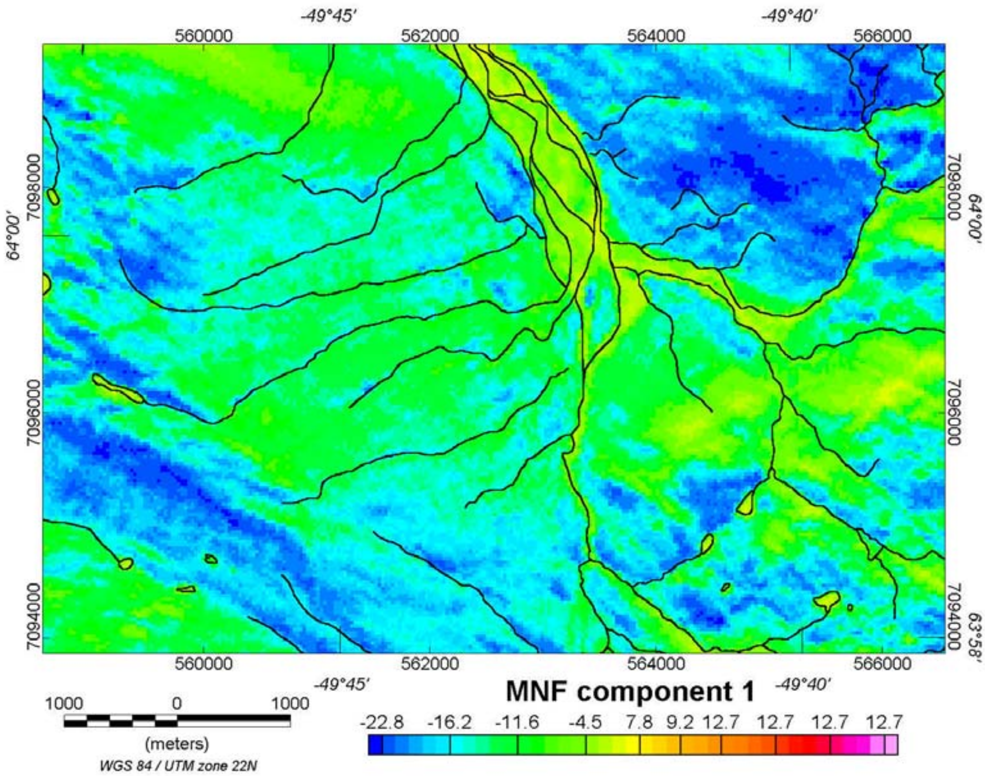

Figure 23. *Component 1 of Minimum Noise Fraction decomposition of ASTER data.*

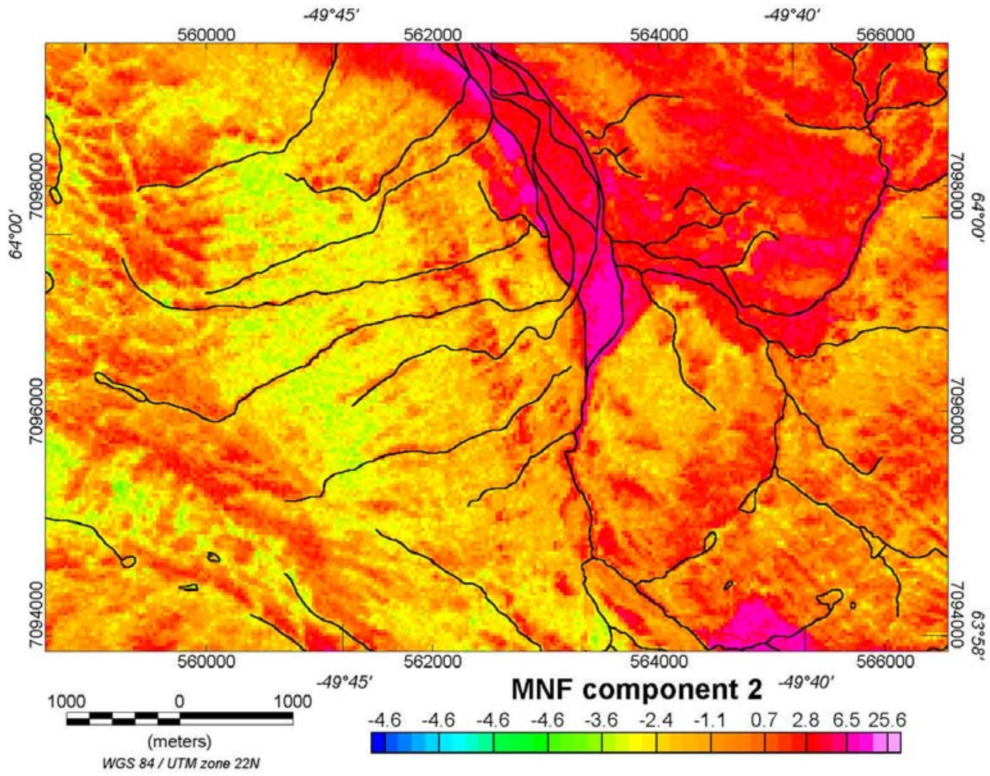

Figure 24. *Component 2 of Minimum Noise Fraction decomposition of ASTER data*

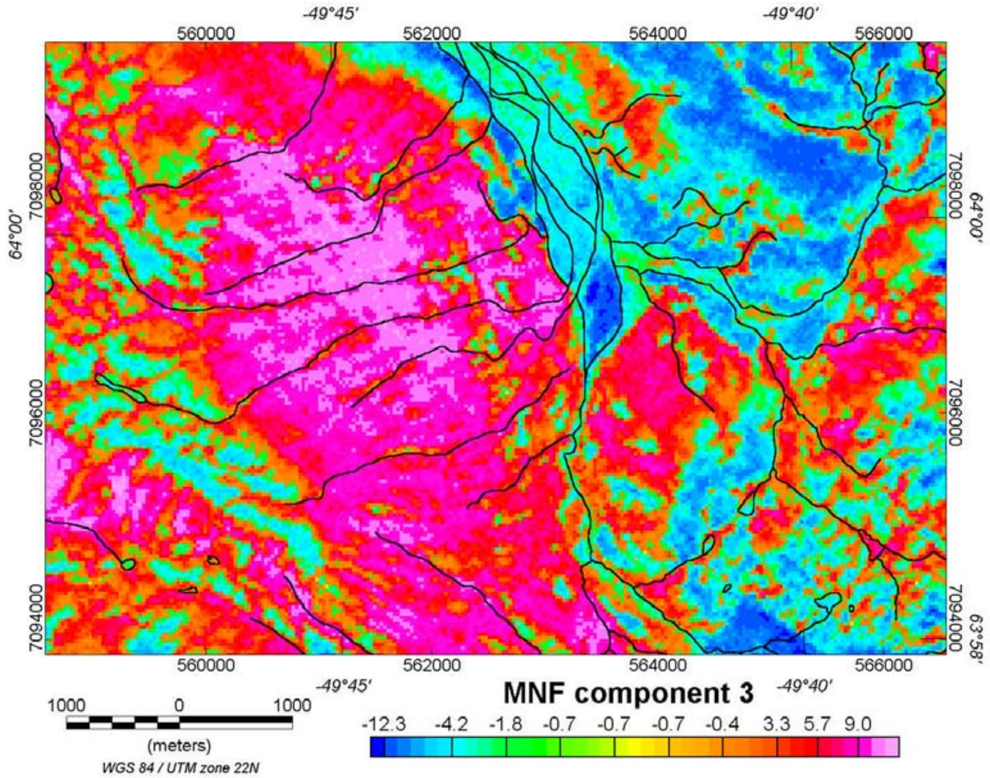

Figure 25. *Component 3 of Minimum Noise Fraction decomposition of ASTER data*

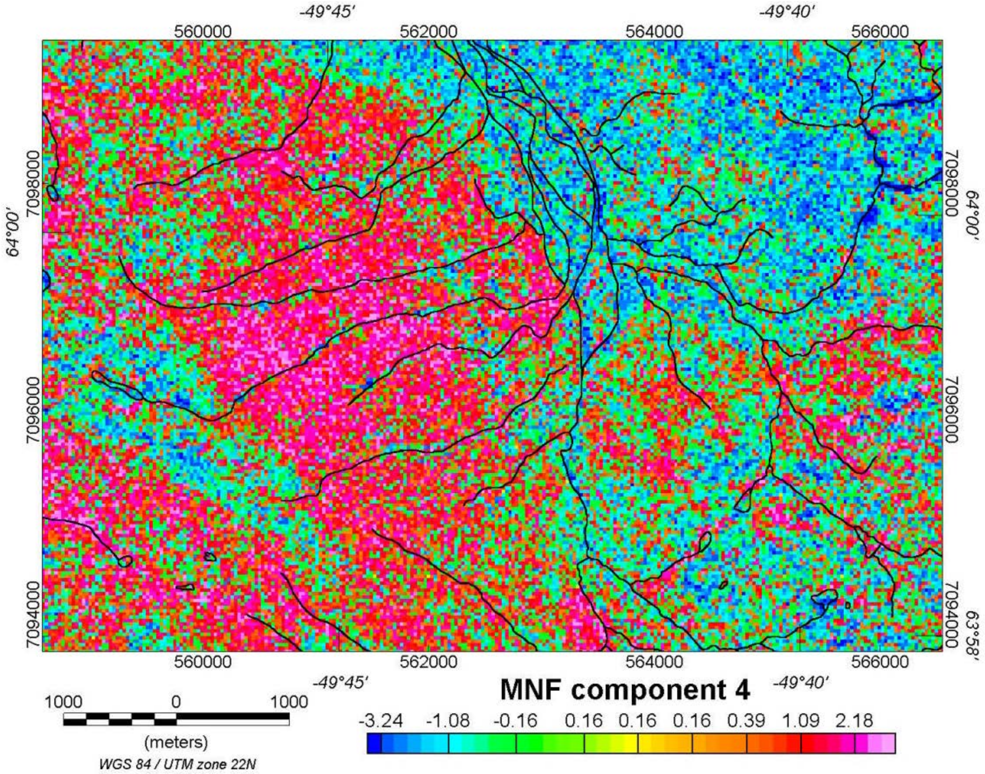

Figure 26. *Component 4 of Minimum Noise Fraction decomposition of ASTER data*

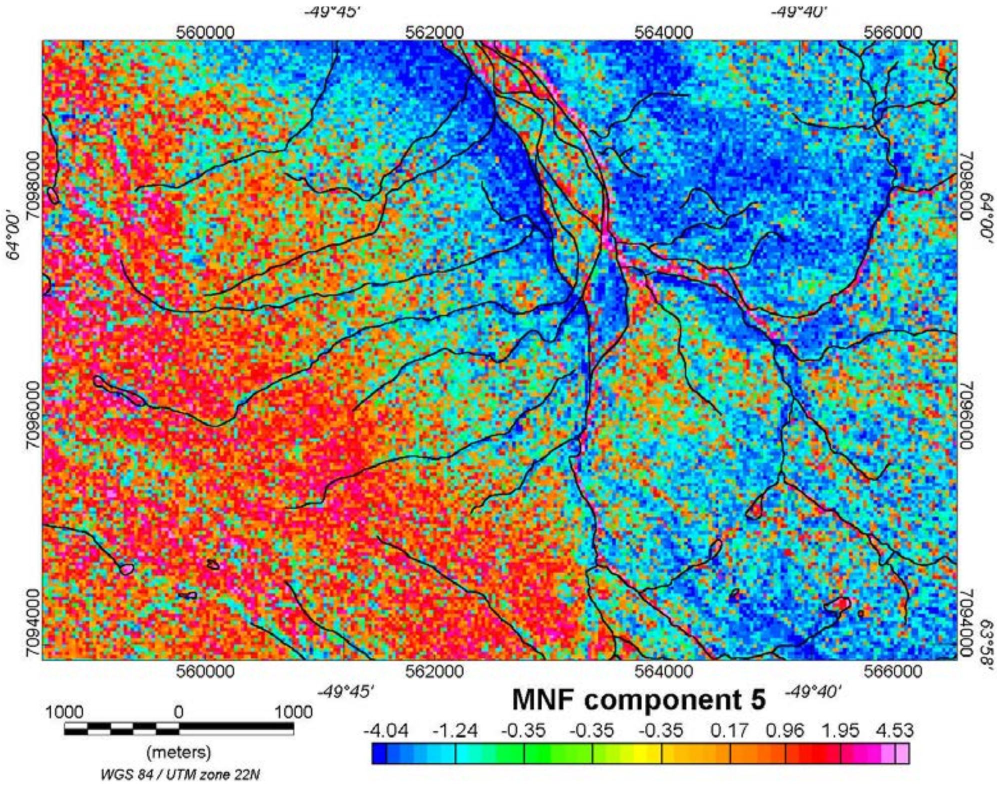

Figure 27. *Component 5 of Minimum Noise Fraction decomposition of ASTER data*

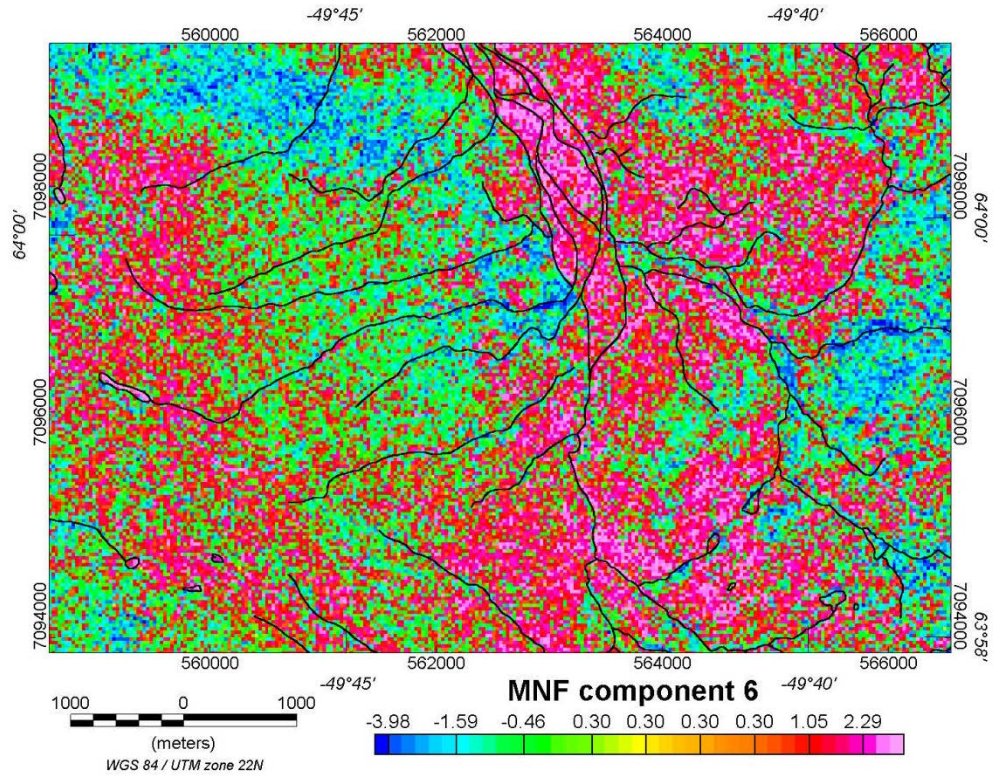

Figure 28. *Component 6 of Minimum Noise Fraction decomposition of ASTER data*

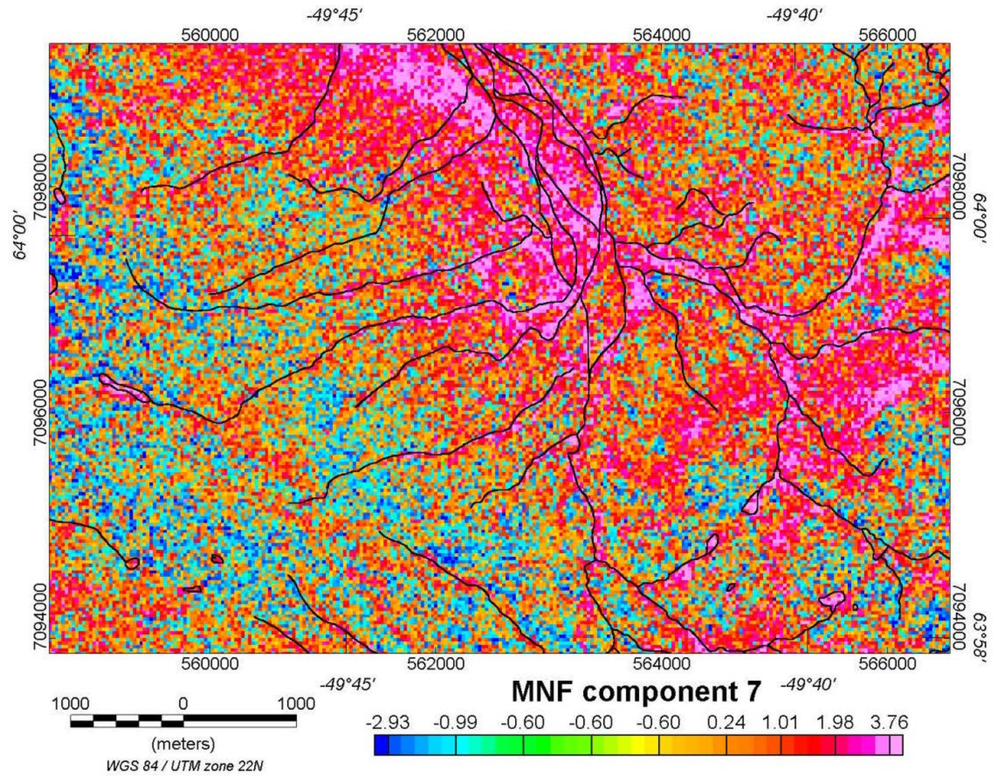

Figure 29. *Component 7 of Minimum Noise Fraction decomposition of ASTER data*

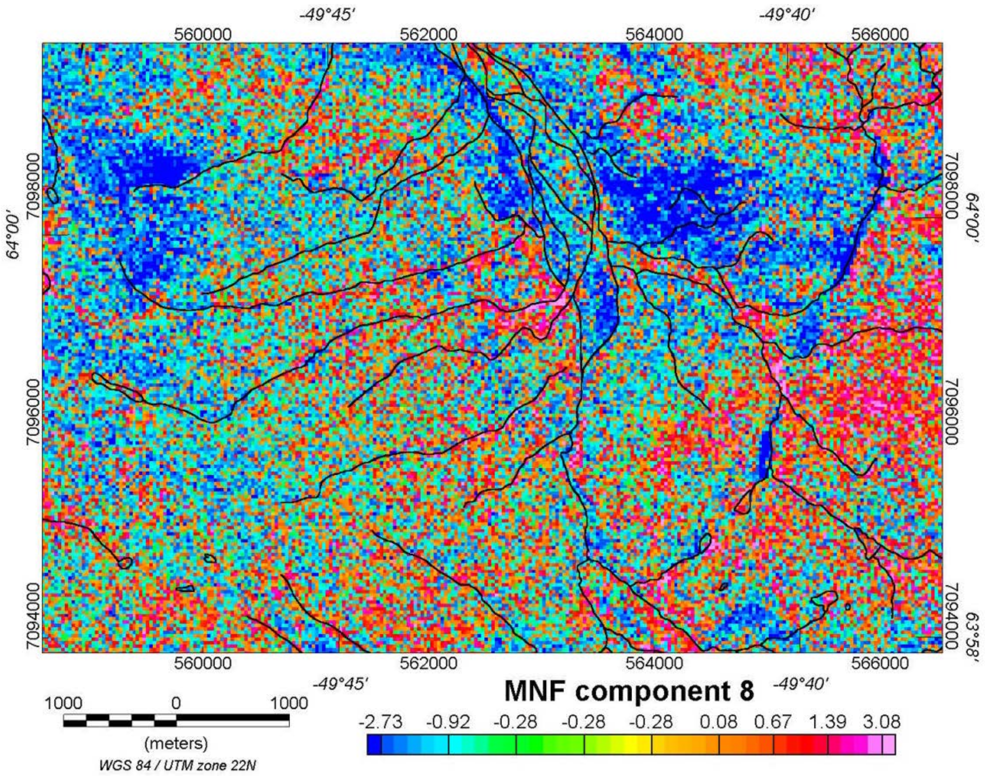

Figure 30. *Component 8 of Minimum Noise Fraction decomposition of ASTER data*

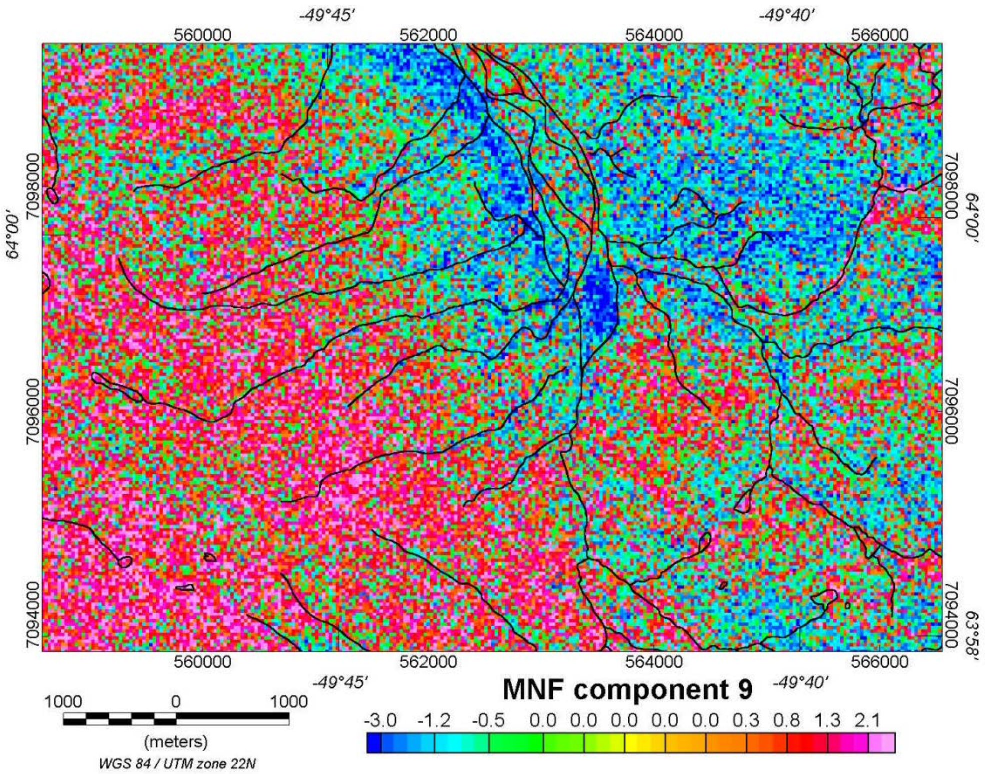

Figure 31. *Component 9 of Minimum Noise Fraction decomposition of ASTER data*

6. Self Organised Map data presentations

Self Organised Map (SOM) presentation of data sets with many data types provide an efficient way of searching for and visualising relationships between different data types. The SOM is furthermore useful for classification and clustering of data. SOM are shown for various combinations of data from the Tikiusaaq geophysical survey in the sections below. A synthetic data set is included in Appendix – Self Organising Maps (SOM) and discussed in order to introduce the method, and describe how the enclosed maps for the Tikiusaaq data can be utilised.

SOM’s are presented using the following combinations of data:

- U, Th, K
- Aster MNF 1-5
- U, Th, K & Aster MNF 1-5
- U, Th, K, Aster MNF 1-5 & second vertical gradient of pseudo gravity field

6.1 Gamma-spectrometry data

The result of the SOM analysis is shown in Figure 32. From the SOM-space presentation and the clustering, it is evident that the areas associated with intermediate to high thorium values define three clusters:

- cluster no. 3 is high in both thorium and uranium
- cluster no. 6 is high in thorium and have intermediate values of uranium. Potassium is noted to have high to intermediate values for this cluster
- cluster no. 2 have intermediate values for both thorium and uranium

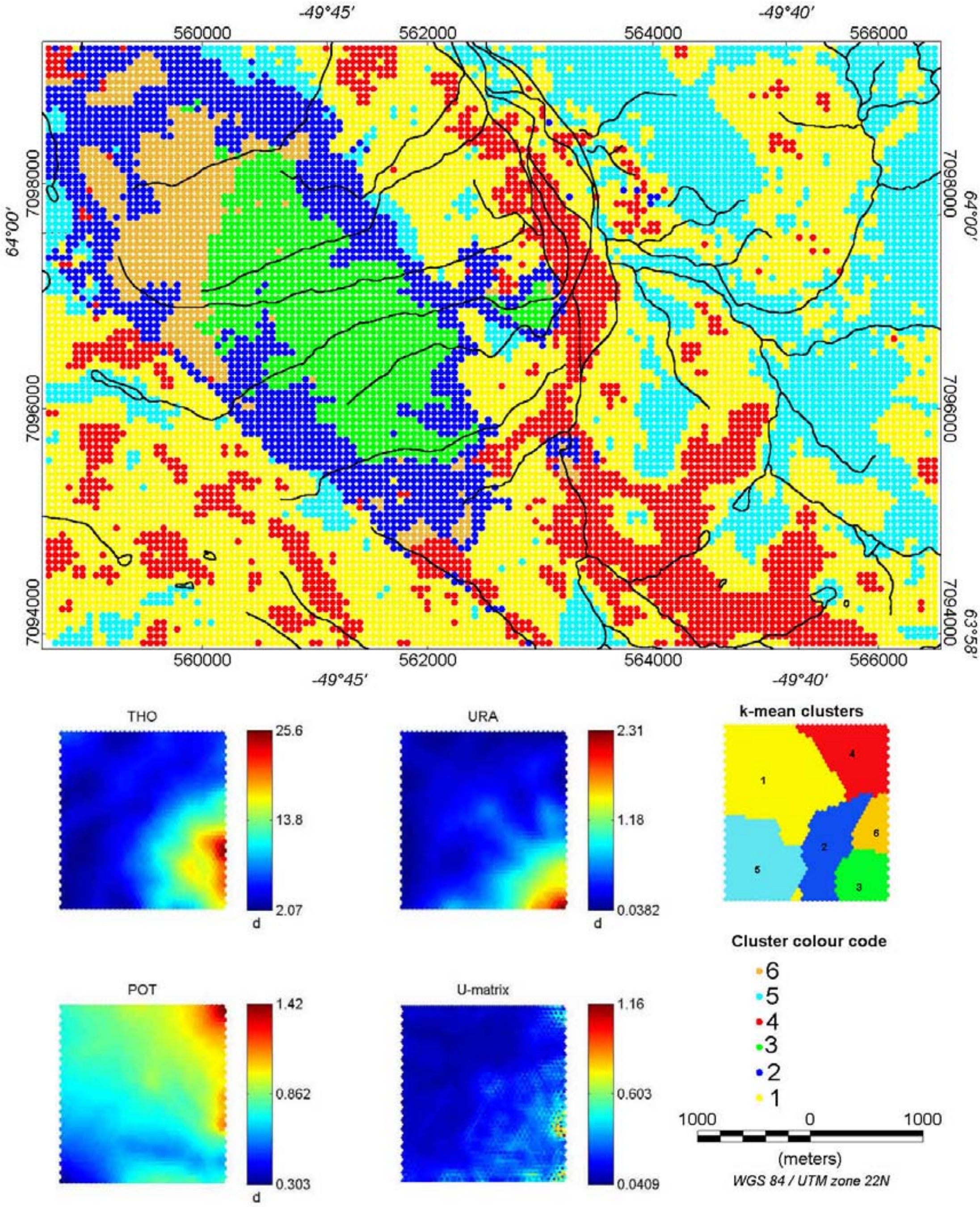

Figure 32. *SOM of gamma-spectrometry data and the results of the k-mean clustering of the BMU's.*

6.2 ASTER MNF components 1–5

The result of the SOM analysis based of ASTER MNF components 1–5 is shown in Figure 33. The most well-defined signature of the ASTER data is associated with the meandering streams in the northern part of the map (cluster no. 4 and 13). Some local variation can be seen within the core of the carbonatite complex (cluster no. 1, 3, 6, 7, 8, 12).

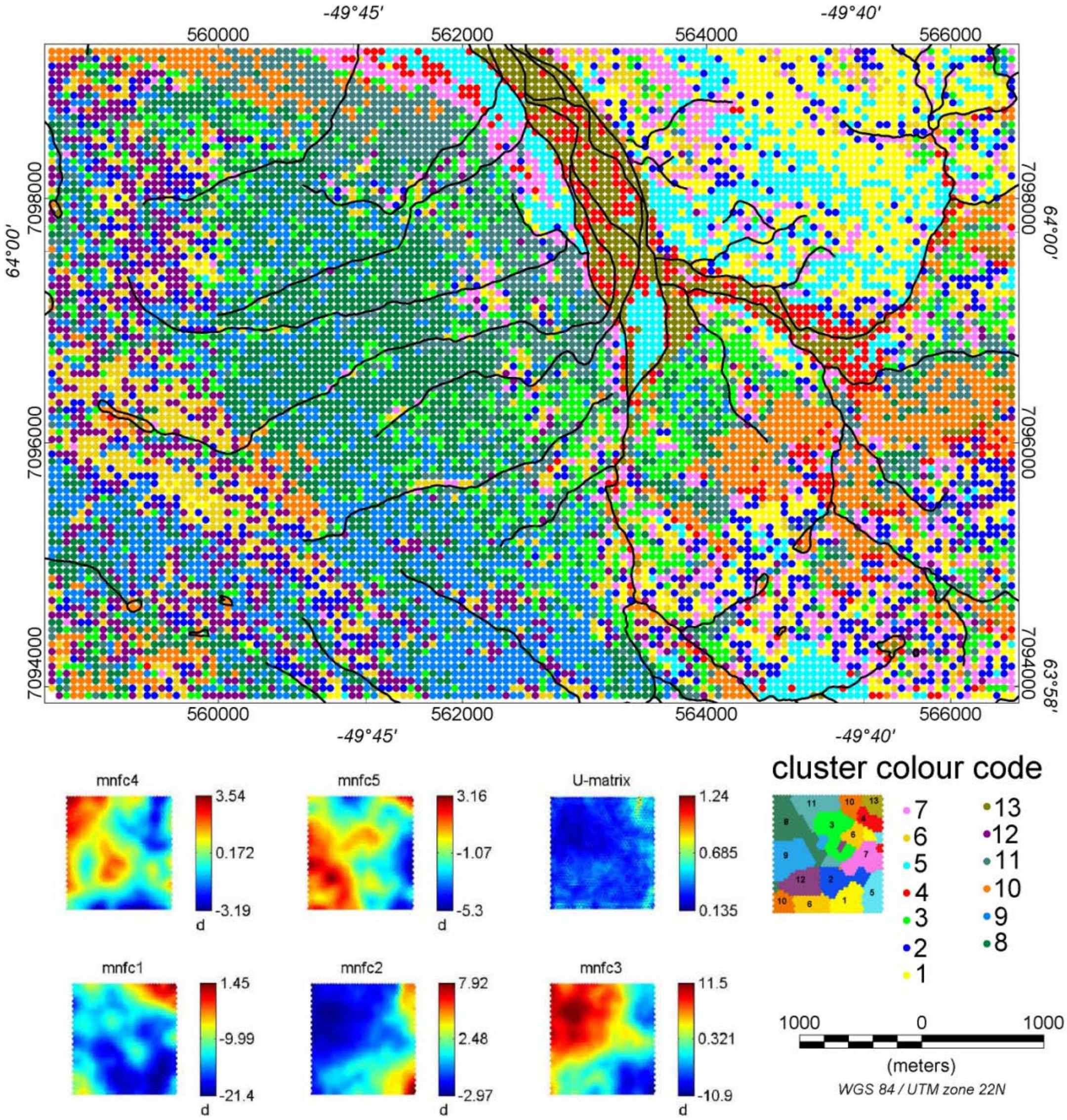

Figure 33. *SOM of ASTER MNF components 1–5, and the results of the k-mean clustering of the BMU's.*

6.3 Gamma-spectrometry and ASTER MNF components 1-5

The result of the SOM analysis of the combined data set with gamma-spectrometry data and ASTER MNF components 1–5 is shown in Figure 34. The similarity to the clustering in Figure 32 indicates that the clustering is controlled mainly by the data characteristics of gamma-spectrometry data. Note that cluster colour code is arbitrary.

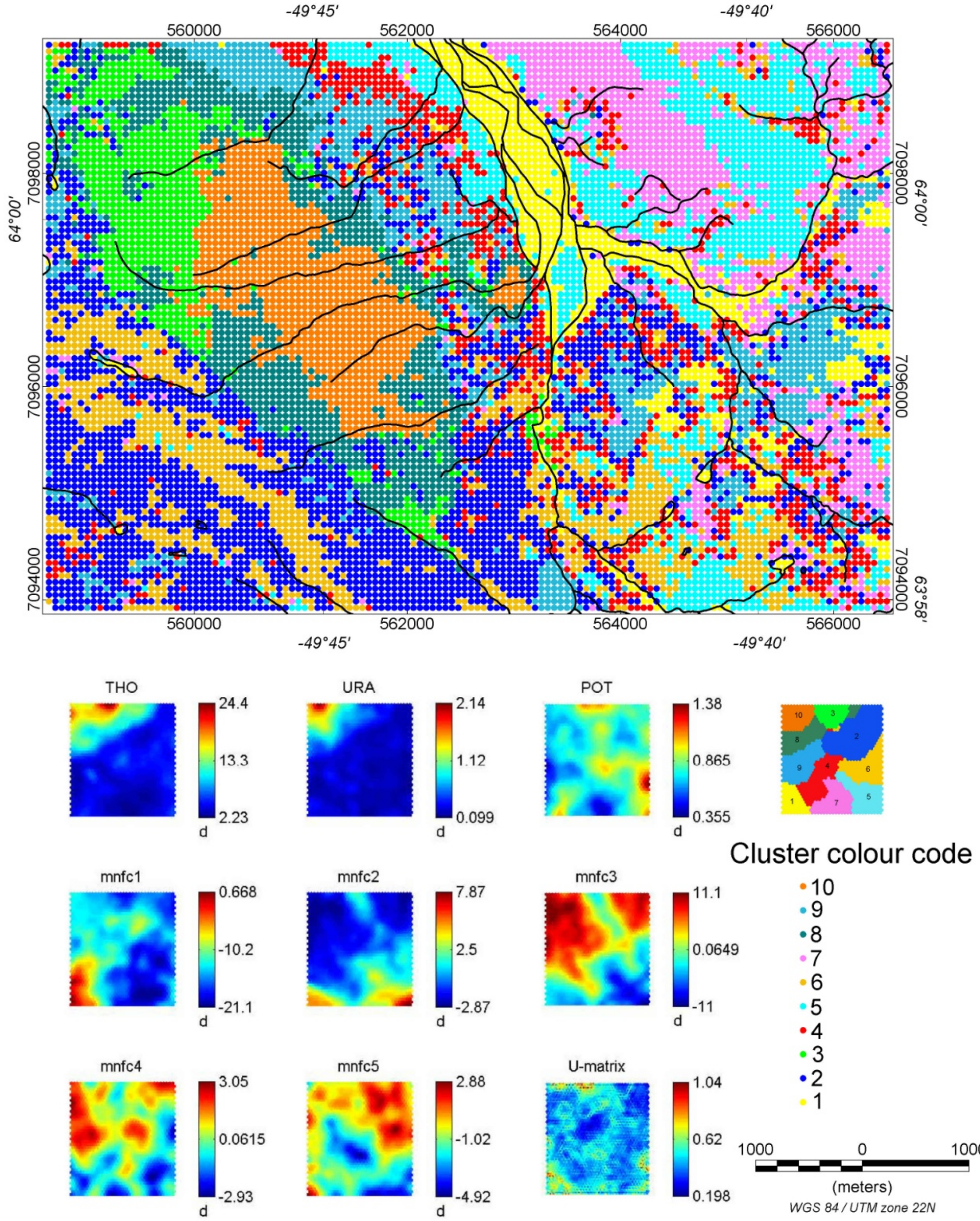

Figure 34. *SOM of gamma-spectrometry data combined with ASTER MNF 1-5 component data, and the results of k-mean clustering of the BMU's.*

6.4 Gamma-spectrometry, ASTER MNF components 1–5 and second vertical gradient of pseudo gravity field

The result of the SOM analysis of the combined data set with gamma-spectrometry data, ASTER MNF components 1–5 and the second vertical gradient of the pseudo gradient field is shown in Figure 35. The inclusion of the second vertical gradient of the pseudo gradient field is seen to add more internal variability within the core complex, when compared to the results with gamma-spectrometry and Aster data combined. The component plots show that peak values of the second vertical gradient of the pseudo gradient field (vg2_PSG in Figure 35) is associated with low to intermediate thorium and uranium values. High potassium values are associated with low magnetisation, but the relationship between potassium and the second vertical gradient of the pseudo gradient field is fairly complex; i.e. areas with low second vertical gradient of the pseudo gradient field are also found in areas with low potassium concentrations.

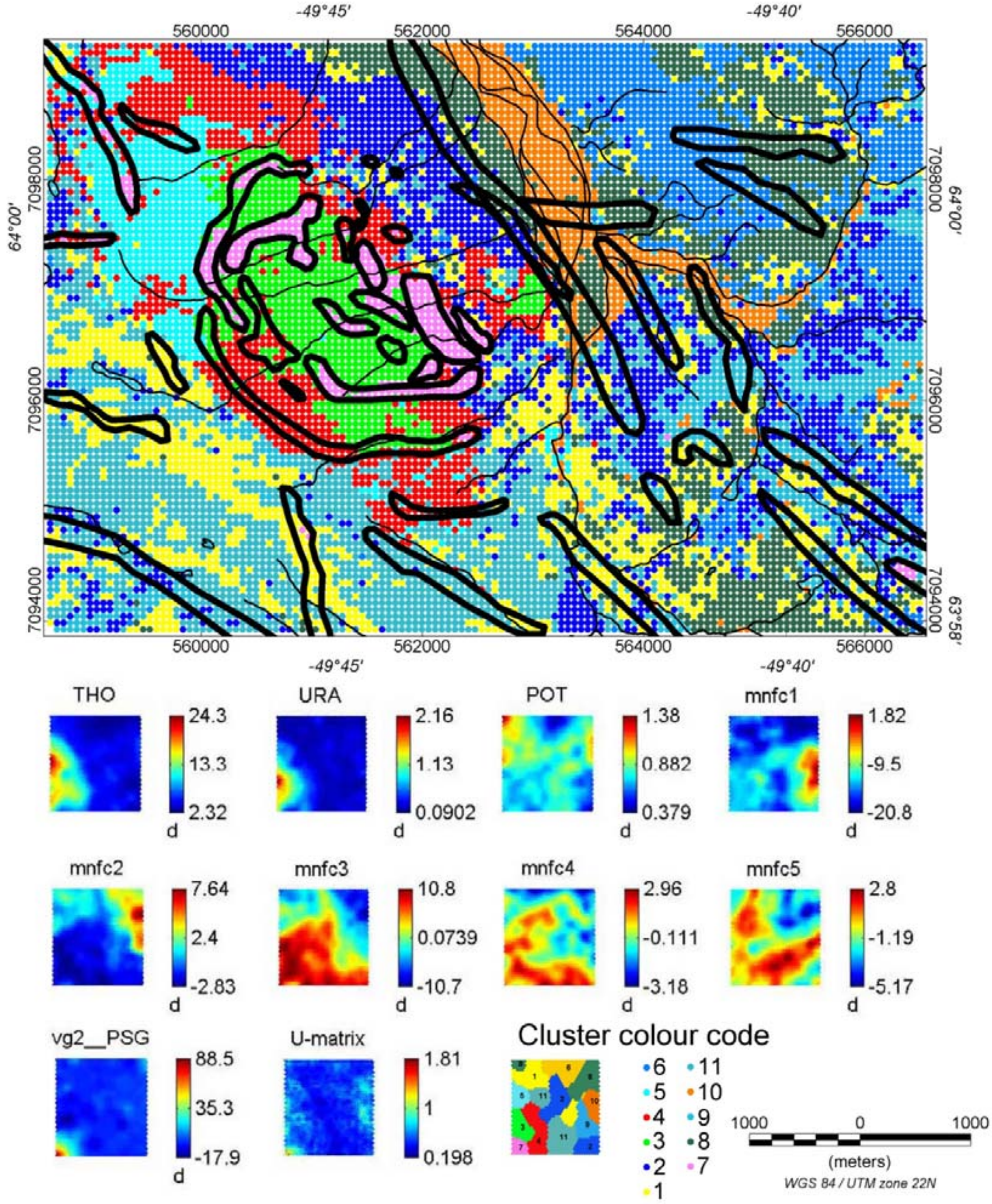

Figure 35. *SOM of gamma-spectrometry, ASTER MNF 1-5 component data and second vertical gradient of pseudo gravity, and the results of k-mean clustering of the BMU's. Polygons outlining approximate locations of highly magnetised structures are superimposed on the image.*

7. Evidence for an enlarged areal extent?

In the discussion on structural information from grid images, it was noted that the area northwest of the Tikiusaaq core complex contains magnetic anomalies that may represent responses from carbonatite related magnetite structures. The evidence for this possible interpretation is discussed here with reference to the data displayed in Figure 36, which shows

a) magnetic total field anomaly
b) horizontal gradient of second vertical derivative of magnetic vertical component (HGSVD)
c) estimated thorium concentration
d) estimated uranium concentration

A 100 m upward continuation was applied to the horizontal gradient of second vertical derivative to suppress short wavelength noise. Locations (from Steenfelt *et al.* 2007) of carbonatite outcrop and subcrop and carbonate veining is marked on the maps in Figure 36. Also locations of dolerite are marked.

Superimposed on the images in Figure 36 are two definitions of the magnetic cores associated with the carbonatite. Thin lines in black colour towards southeast embraces the response from the previously Tikiusaaq carbonatite discovery. The outline is here based on the 2010 magnetic survey. A second polygon defined here by black lines that merge with the minor polygon represents an interpretation with a further increase in volume. The larger polygon are drawn after visual inspection of the HGSVD data in Figure 36c. In favour of this new interpretation of the carbonatite complex is that both the thorium and uranium concentrations are high within the outlined area. In particular it is noted that the large polygon enclose the peak thorium anomaly. Another observation in favour of an enlarged extend of the carbonatite is the coherently low magnetic area north of the proposed core complex.

An argument against the above mentioned extension of the carbonatite core complex is that they are inconsistent with the mapped geology (GEUS, Geologisk kort over Grønland, Kapisillit 64 V.2 Syd). This discrepancy could simply be a matter of depth to the intrusion; i.e. no exposures exist, or could be a matter of less dense and smaller amount of carbonatite occurrences. A few locations with carbonate veining is seen within the enlarged extent and two location with exposure of carbonatite is reported within about 500 and 1000 m west of the polygon outlining the initial core complex.

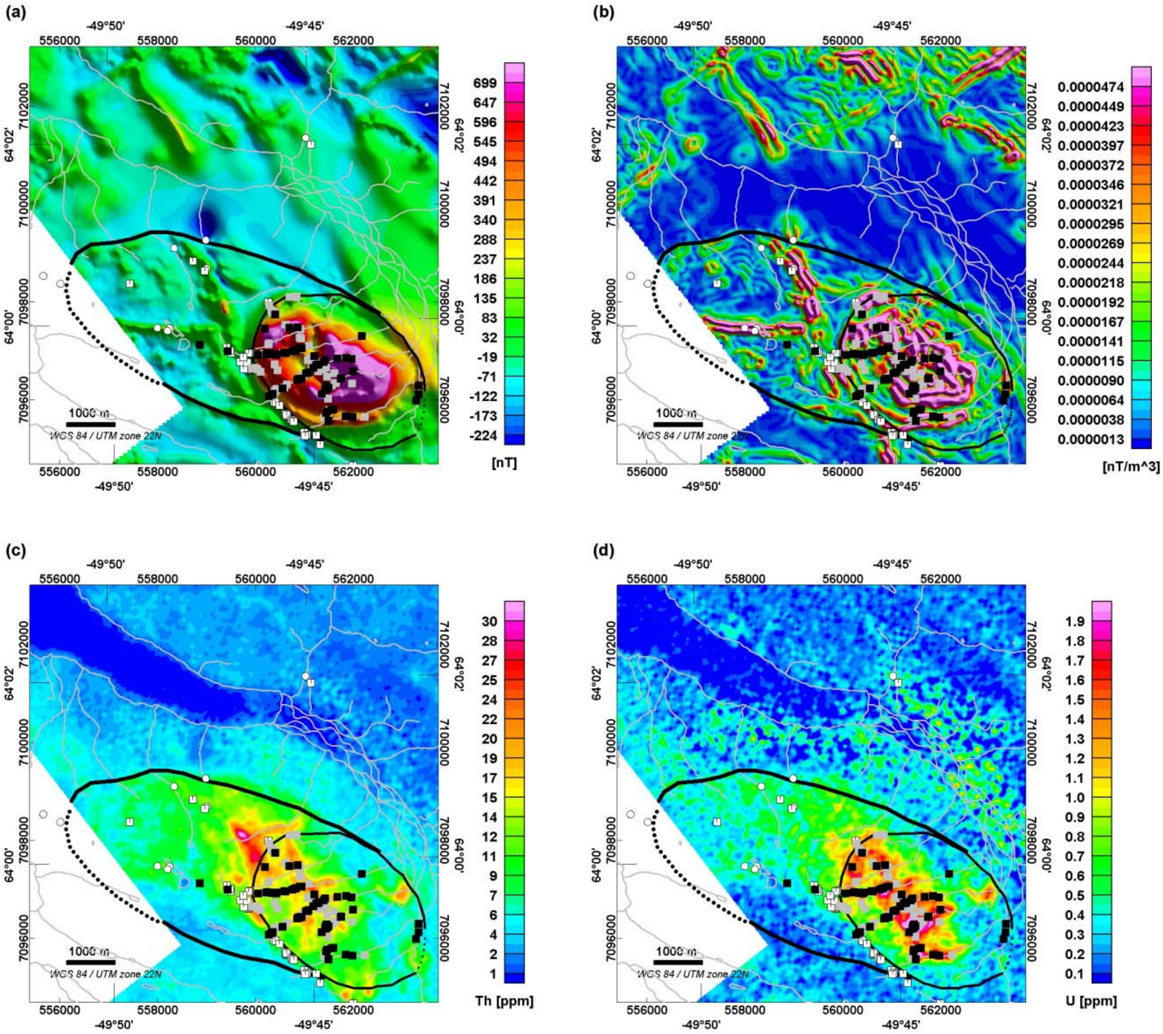

Figure 36. *Images of (a) magnetic total field anomaly; (b) horizontal gradient of second vertical derivative of magnetic field; (c) estimated thorium concentration and (d) estimated uranium concentration. Two possible interpretations of the carbonatite (magnetic) core extend are outlined by polygons in black colour. Location of dolerite sills are marked by white circles with black circumference; localities with carbonatite outcrop and subcrop are marked by black and grey square boxes respectively and localities with carbonate veining are shown by white square boxes with black circumference.*

8. Conclusion

The main result of the analysis of the geophysical data is the interpretation that the highly magnetic bodies associated with the carbonatite core complex extent to large depth (500 m). It must however be kept in mind that interpretation of magnetic data is ambiguous, and the interpretation should be used with some caution. Inclusion of information from independent geological field observations should be utilised in order to add more confidence to the interpretation. In particular, description of the degree of inhomogeneity of the magnetite outcrop in combination with in-situ measurements of the magnetic susceptibility would be useful for an improved interpretation. Ground magnetic profiling is expected to add useful data if this is combined with in-situ descriptions of surface geology.

The individual MNF components contain information about spatial variation of the surface properties. In particular, component 2-4 contains useful information on the regional properties. Higher components show more scatter but may contain useful local information.

The gamma-spectrometry data are very useful for a classification of the area. The SOM analysis of the gamma-spectrometry data indentifies three clusters within the carbonatite core complex. The ASTER MNF data contains some localised anomalies which result in a SOM with more variability compared to the SOM based on gamma-spectrometry only. The magnetic data are not showing a clear linear correlation to the gamma-spectrometry and ASTER MNF data. The magnetic data essentially contributes by subdividing the clusters derived from the gamma-spectrometry and ASTER MNF SOM. High magnetic fields within the core complex are mainly associated with areas of intermediate to low values of thorium and uranium.

The larger spatial variability of clusters or spatial inhomogeneity associated with the ASTER MNF SOM may be linked to a significant dependency of these data on local spatial features such as occurrence of vegetation. Gamma-spectrometry data are much less influenced by vegetation.

A comparison with the lithology mapping (Figure 37) presented in Steenfelt et al. (2007) does not reveal a simple relation between the obtained clusters from the SOM analyses and the mapped geology. Refining the SOM analysis by using smaller amount of data might turn out to be useful for correlation to mapped geology, but this has not been attempted for this report. Expansion of the SOM by incorporation of geochemical data may also be useful.

Several local and regional scale lineaments can be extracted from the magnetic data. Within the carbonatite core complex, the majority of the magnetic structures associated with the lineaments show dips outwards and away from the centre of the complex.

A possible interpretation with a much larger extent of the carbonatite complex than estimated initially should be investigated further. Geological observations are in general not in favour of this interpretation, but some carbonatite exposures are reported within the expanded area.

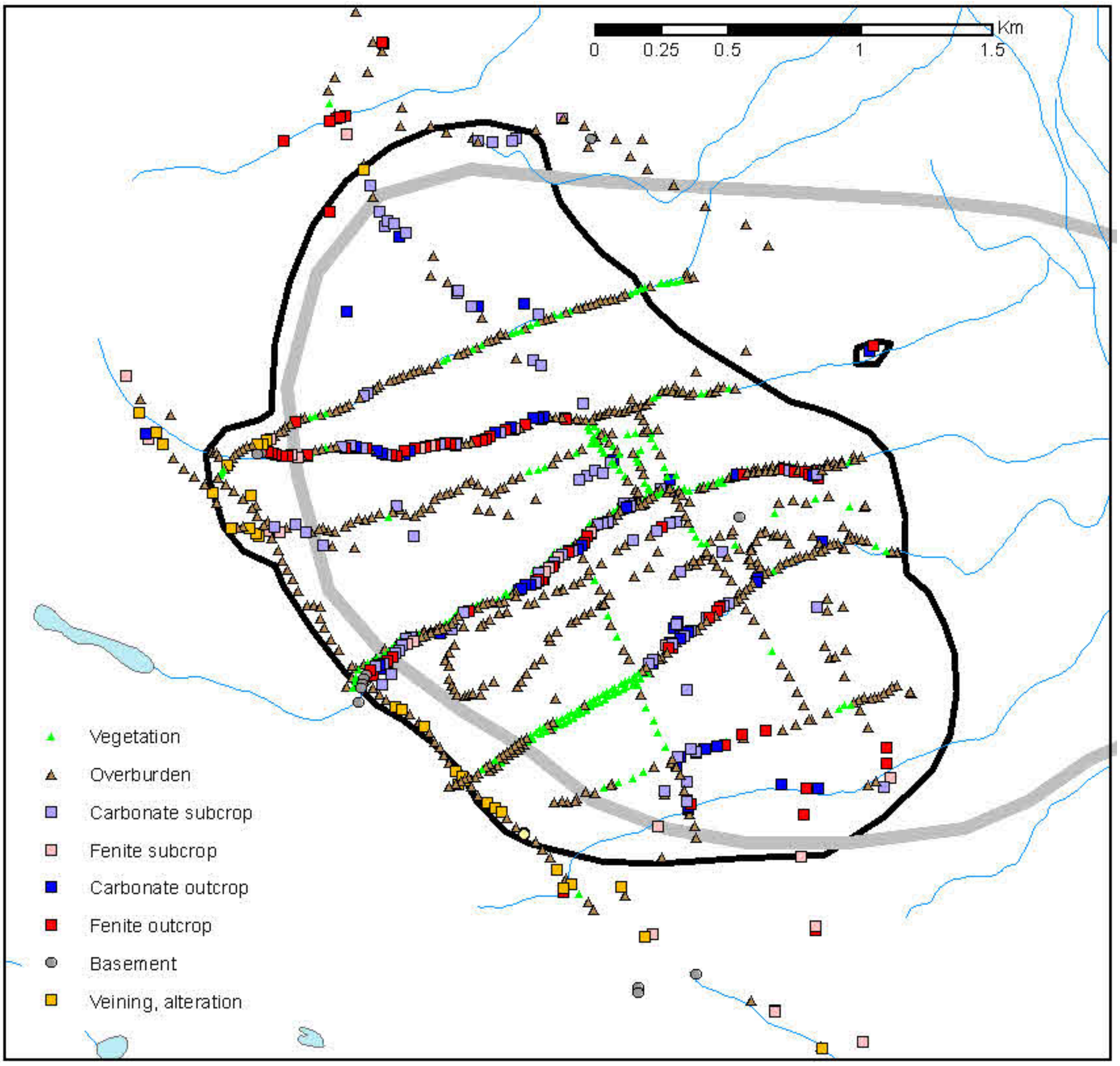

Figure 37. *Lithology of carbonatite core area from Steenfelt et al. (2007). The polygon in dark grey colour outlines the magnetite core as defined by Steenfelt (2007). The polygon in black colour outlines the core defined from outcrop of carbonatite.*

9. References

Barnes, G.B. 2000a: Sarfartoq, Exploration License 25/96. Internal report, New Millenium Resources NL, 8 pages, 8 appendices, 2 plates (in archives of the Geological Survey of Denmark and Greenland, GEUS Report File 21768).

Barnes, G.B. 2000b: Qaqqaarsuk Exploration Licence. Internal report, New Millennium Ressources NL, 27 pages, 6 appendices, 2 plates. (in archives of the Geological Survey of Denmark and Greenland, GEUS Report File 21769).

Fraser, S.J. & Dickson, B.L., 2007: A New Method for Data Integration and Integrated Data. Interpretation: Self-Organising Maps. In "Proceedings of Exploration 07: Fifth Decennial International Conference on Mineral Exploration" edited by B. Milkereit, 2007, p. 907-910.

Green, A.A., Berman, M., Switzer, P. & Craig, M.D. 1988, A Transform for Ordering Multispectral Data in terms of Image Quality with Implications for Noise Removal. IEEE Trans. Geosci. Remote Sens., vol. **26**, No. 1, pp. 65–74.

Kohonen, T, 2001: Self-Organizing Maps. Third Extended Edition, Springer Series in Information Sciences, Vol. 30, Springer, Berlin, Heidelberg, New York, 2001.

Steenfelt, A., Hollis, J.A. & Secher, K. 2006: The Tikiusaaq carbonatite: a new Mesozoic intrusive complex in southern West Greenland. Geological Survey of Denmark and Greenland Bulletin **10**, 41–44.

Steenfelt, A., Schjøth, F., Sand, K.K., Secher, K., Tappe, S., Moberg, E. & Tukiainen, T.2007: Initial assesment of the geology and economic potential of the Tikiusaaq carbonatite complex and ultramafic lamprophyre dykes. Danmarks og Grønlands Geologiske Undersøgelse Rapport **2007/64**, 53 pp + 1 DVD.

10. Appendix - Self Organising Maps (SOM)

Three data types, d1, d2 and d3, are analysed in the example with synthetic data. The data values and geographic locations are shown (Fig. 38abc) for each data type using a colour code presentation for each data point value. The values are in the range from 1–16. In short the data fall in four sub ranges:

- Very low (VL) – blue colour
- Low (L) – light blue and green colours
- Intermediate (I) – orange colour
- High (H) – purple colour

A listing of the three data types in terms of sub ranges reveals the following combinations from south (1) to north (4) when inspecting the three data types in Fig 32abc:

1. VL-L-L
2. VL-I-L
3. L-L-L
4. VL-L-H

The listing above give four different combinations of data and it is clear immediately that the data define four groups. In this simple synthetic example with only a few types of data, it is straightforward to distinguish the four groups. However, an analysis by visual inspection becomes much more difficult when both more data types and more complex data distributions are added. The SOM is useful in these complicated cases. The basic principles are described below.

The SOM processing finds an approximation to the data by mapping the input data into another data set with fewer data than the initial amount of data. This approximation referred to as the best matching units (BMU) has the same amount of data types (same dimensionality) as the input data. The BMU's are presented in the SOM which is a two-dimensional map, and referred as the SOM-space (see Fig. 38 lowermost panels). The SOM is discretized in a pre-selected number of rows and columns (matrix-representation). Thus, the original multi-dimensional data are mapped into a new data space with only two-dimensions and fewer data. In the synthetic example, the number of rows and columns are 21 and 16 respectively. The number of cells or elements defines the data reduction applied to the initial data. In this synthetic case, a reduction from 998 initial data to 21x16=336 data is used. Each BMU is associated with a cell in the matrix or SOM-space, and they are ordered in the matrix such that similar BMU's are adjacent to each other in the two-dimensional map. Although the SOM is two-dimensional, the multidimensionality of the input data is retained by the dimensionality of BMU. Each of the input data has a BMU to which the data are most similar to. Several input data may be associated with the same BMU, in which case the SOM presentation may be viewed as a classification of the input data. An example of a link between initial data and a BMU is indicated in Figure 32, where six data points are represented by one BMU in the matrix. Some BMU's may not have any of the initial data associated to it. The matrix presentation is utilised in two ways:

- U-matrix presentation: similarity between adjacent BMU's

- Component presentation: relationship between components for subsets (i.e. data associated with one or several cells in the matrix) of the data

The U-matrix describes the deviation for a particular cell to the surrounding cells by using a colour scale representation of the “distance” between the associated BMU’s. The component presentation simply shows the value of the BMU at each cell and for each component.

The BMU’s may be analysed further with respect to clustering of data. A standard k-mean clustering procedure is used. The result for the synthetic data example is that the data cluster into four distinct groups, as displayed in Figure 38d. Thus, a data reduction or simplification from 998 initial data to 4 is obtained.

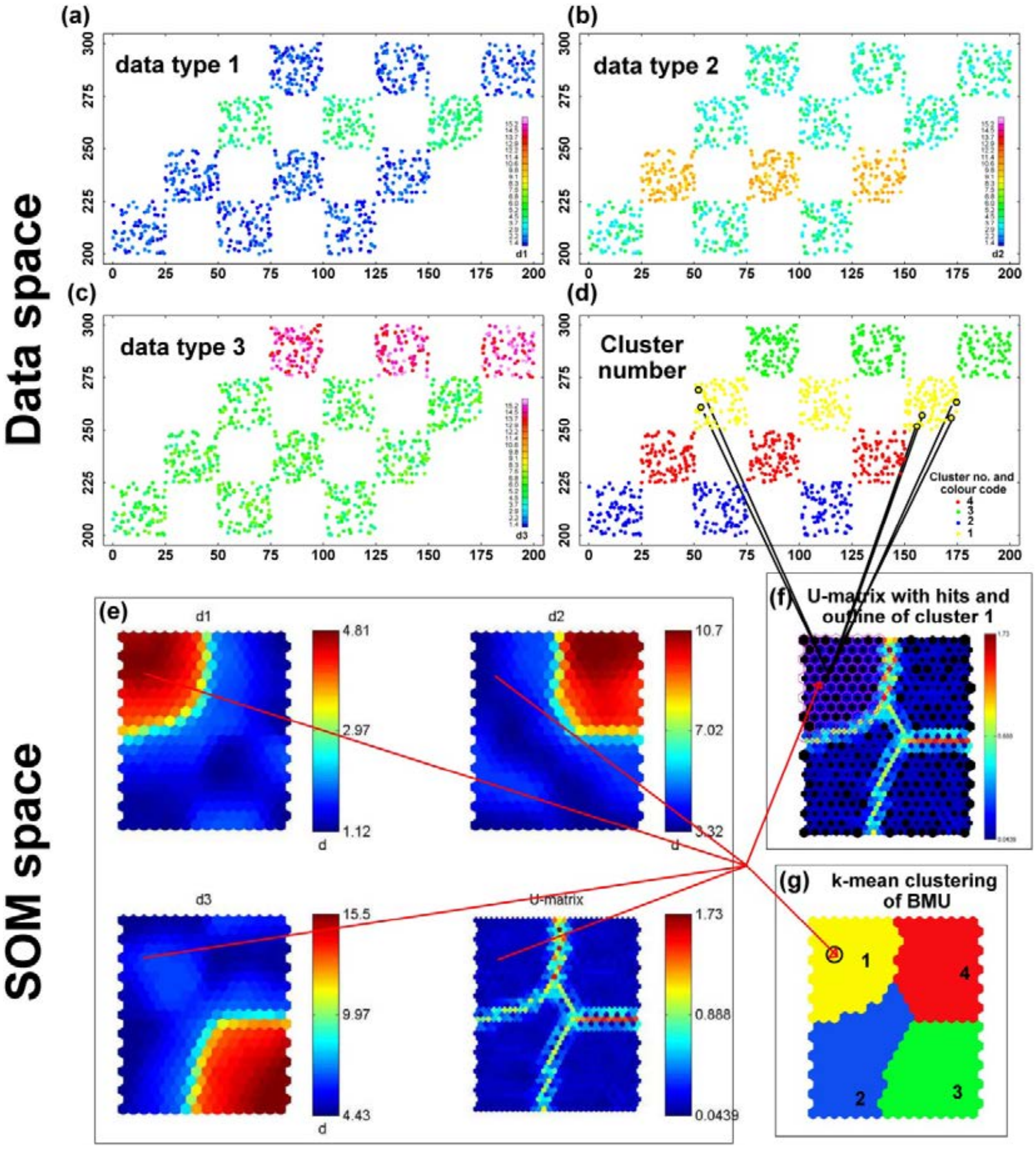

Figure 38. *SOM-presentation of synthetic data consisting of 998 locations with 3 data types at each position: (a) values of data type d1 at each geographic location; (b) values of data type d2; (c) values of data type d3; (d) results of k-mean cluster analysis displayed in a geographic map ; (e) components in SOM-space; (f) U-matrix representation of BMU with colour code showing distance to neighbouring cells; (g) k-mean clusters of BMU’s in SOM-space. An example of link between data space and SOM-space is indicated by the lines pointing to one of the cells in the matrix representation.*